$\gamma\gamma$ AND $e\gamma$ COLLISIONS AT FUTURE HIGH ENERGY COLLIDERS

J.H. FIELD *
L.P.N.H.E. Université Pierre et Marie Curie
4, Place Jussieu - F75230 Paris

ABSTRACT

After briefly reviewing previous work on two photon collisions at future high energy colliders (e^+e^-, e^-p, pp, $p\bar{p}$) a comparative survey is made of PETRA, LEP, SLC and HERA from the view points of luminosity, acceptance and energy range. A more detailed study is then presented of a 0° tagging system in the proton beam line of HERA. Bremsstrahlung background and the separation of two photon production and diffractive electroproduction events are briefly discussed. It is concluded that HERA gives a unique possibility to study single and double tag two photon physics for large centre of mass energies > 10 GeV.

The interest of observing $W^{\pm}$ and Z^0 production in virtual photon e, p collisions at HERA is also mentioned.

In the second part of the talk, devoted to the more distant future, the possibility of producing real $\gamma\gamma$ or γe collisions in very high energy linear colliders such as SLC or VLEPP is discussed. Both the technical realisation, by Compton back scattering of high intensity laser beams, and the new domain of physics which would be opened to experiment are considered. Large rates of single Z^0 and $W^{\pm}$ production are expected in γe collisions well as measurable rates for W^+W^- pair production in $\gamma\gamma$ collisions. The W production cross sections are sensitive to the fundamental gauge boson vertices γWW and $\gamma\gamma WW$.

---

* On leave of absence from DESY Hamburg.

I. INTRODUCTION

A list of some future (and existing) collider projects is given in TABLE 1. This list, though certainly not exhaustive, is at least representative as it contains examples of all types of colliders forseen until now :

(i) e^+e^- storage ring

(ii) $e^{\pm}e^-$ one pass linear collider

(iii) $p\bar{p}$ single ring collider

(iv) pp double ring collider

(v) ep double ring collider

A priori,two photon physics is possible at any collider, though all experimental results published till now (with one exception) have come from e^+e^- storage rings. By far the largest number of studies have been devoted to the LEP machine [1],[2],[3] , [4], [5] . For a comprehensive survey of the various physics topics accessible at LEP the interested reader is referred to Davier's contribution to the 1981 Paris two photon workshop [5] . No further discussion will be given here except to compare in a global way LEP with PETRA, SLC and HERA with respect to luminosity and energy range.

The linear colliders (ii) such as SLC [6] and VLEPP [7] are of interest not so much for "classical" 2γ physics using virtual photons but because of the unique possibilities they offer for generating high intensity real photon beams (in arbitary polarisation states) which may be used to make very high energy ($W > 100$ GeV) real $\gamma\gamma$ and $e\gamma$ collisions. The technique used to generate the real photon beams, as well as the new physics topics which can be investigated by their use, are discussed below in sections 6 and 7. In these sections I have drawn largely from previous work carried out both at SLAC [8] and Novosibirsk [9] [10] [11] on the technical problem of generating the real photon beams by Compton back scattering of Laser beams. This subject has also been reviewed by Kessler [12] . For the physics of very high energy γe and $\gamma\gamma$ collisions the work of Renard [13] and Ginsberg et al [14] has largely been used.

Two photon physics in pp and $p\bar{p}$ collisions has been reviewed from the theoretical view-point by Donnachie [15] and from the experimental one by Tao [16]. Most theoretical work has been devoted to calculations [17] , [18] , [19] of the background due to the 2γ process $pp \to \mu^+\mu^- pp$ in the Drell Yan [20] production of μ pairs. One experiment at the ISR [21] has detected 2γ production of $\mu^+\mu^-$ pairs in pp collisions (this is the "exception"referred to above). More recent calculations of $\mu^+\mu^-$ production in pp, $p\bar{p}$ and ep collisions have been performed by Vermaseren [22] .

As for the production of hadronic final states in 2γ collisions with pp or $p\bar{p}$ colliders it has been generally concluded [15], [16], [23] that the two photon collision processes would be completely overwhelmed by pomeron-pomeron fusion (Fig. 1a) or by double gluon exchange graphs (Fig. 1b). It is interesting to note that, as already pointed out by Sens [24], the experimental data from the I.S.R. [25] on the reaction pp → ppX, where the scattered protons are detected at small scattering angles ($t \simeq 0.1$ (GeV/c)^2) do not indicate dominance of pomeron pomeron scattering as suggested, for example, in Ref. [15]. The observed mass spectra for the system X at total centre of mass energies of 23 and 30 GeV/c^2 (Fig. 2) show no dominant production of states of spin parity 0^+, 2^+, ... (for example f_o) as required for pomeron pomeron fusion . Rather, copious production of ω_o, ρ_o, A_2 is seen. There is a small f_o signal. Since however the f_o cross section shows the same energy dependance as

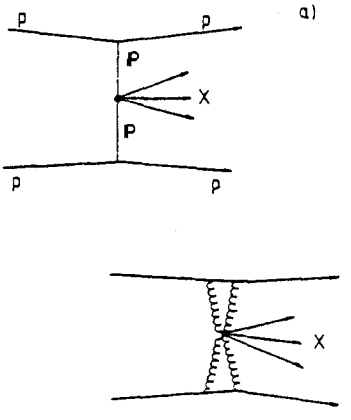

Fig. 1 - a) Pomeron pomeron fusion graph.
b) Double gluon exchange graph.

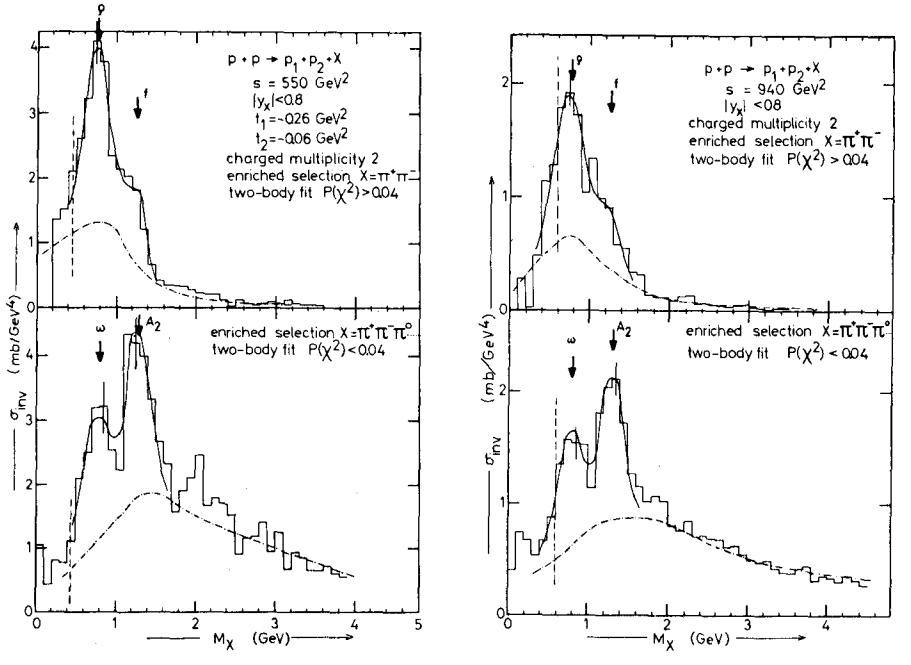

Fig. 2 - Missing mass spectra of the reaction p + p → p + p + X. ISR experiment Ref. [25]. The dash-dot line indicates the estimated non-resonant background.

the ρ_0, ω_0 production it can not be produced predominantly by pomeron pomeron fusion. It may turn out that the pomeron, which is a useful concept for describing diffractive scattering in the language of Regge-pole exchange, has little relevance in processes such as that show in Fig. 1a. Because of the short range $\simeq$ 1f (or equivalently large momentum transfer $\simeq$ 1 m_π) associated with confinment effects in QCD the importance of a two double gluon exchange graph such as that shown in Fig. 1b in the very low t region where one or both protons are elastically scattered is unclear. To the writer's knowledge no QCD calculations of such processes have so far been attempted.

Before leaving the subject of pp and $p\bar{p}$ collisions the essential conclusions of Ref. [16] may be restated. A very high luminosity pp collider such as the original ISABELLE project would have $\simeq$ 2X the LEP luminosity for two photon physics in the region of energy overlap and a much larger energy range (W_{MAX} = 800 GeV/c^2 compared to 260 GeV/c^2). Because of the unknown level of purely hadronic background processes such as these indicated in Fig. 1a, 1b it was concluded that 2γ collision events may be difficult to isolate, but that the hadronic background processes are themselves of considerable physical interest. In contrast the luminosity of the CERN $p\bar{p}$ collider and the planned fermilab $p\bar{p}$ collider are too low to be of any interest for two photon physics, except perhaps for the detection of the 2μ final state as a luminosity monitor.

The writer's opinion is that 2 photon physics remains a very interesting option for a high luminosity pp collider. The separate lattices of the two colliding proton beams contain horizontal bends which, as in the case of HERA (see below) can be used to facilitate 0° tagging. My guess is that processes such these shown in Fig. 1a,b will not constitute an overwhelming background, in any case, for the 2 photon events of the greatest physical interest e.g. those with high transverse momentum jets, or exclusively produced meson pairs in the final state.

The possibility of using an ep collider to study 2γ collisions was first suggested by Coignet [26], and was briefly considered also by Kessler [23]. Now that the HERA proposal [27] is available a more quantitative re-appraisal of its potential for two photon physics is possible. In Section 2 below the luminosity and available kinematic range of HERA are compared with PETRA, LEP and the SLC while in Section 3 a first study is made of 0° tagging in the proton beam line. In both cases the conclusions reached are encouraging and indicate the interest of further, more detailed studies. Section 4 contains estimates of the background due to diffractive electroproduction processes and beam-beam bremsstrahlung in the proposed 0° tagging system. In Section 5 some estimates of the production rate of Z° and $W^\pm$ bosons in γ e and γ p collisions at HERA are briefly reviewed.

2. A COMPARISON OF PETRA, LEP, SLC AND HERA

To make a realistic comparison of an existing machine (PETRA) with the proposed LEP, SLC and HERA colliders an effective luminosity (arbitrarily taken to be $\frac{1}{3}$ of the design luminosity) is assumed for LEP, SLC and HERA while the luminosity measured over a 65 day run is taken for PETRA.

The collision energies and effective luminosities $\bar{\mathcal{L}}$ are then as indicated in Table 2.

Using the equivalent photon approximation, the two photon luminosity differential in the effective mass W of the colliding 2γ system can be written as :

$$\frac{d\mathcal{L}^{tot}_{\gamma\gamma}}{dW} = \frac{dL}{dW}\,\bar{\mathcal{L}} \qquad (1)$$

Where $\frac{dL}{dW}$ is a differential two photon luminosity function given by :

$$\frac{dL}{dW} = 4\left(\frac{\alpha}{\pi}\right)^2 \frac{1}{W} \ln\left(\frac{2E}{m_1}\right) \ln\left(\frac{2E}{m_2}\right) f\left(\frac{W}{2E}\right) \quad \ldots \qquad (2)$$

where $f(z) = (2+z^2)^2 \ln\frac{1}{z} - (1-z^2)(3+z^2) \simeq 4 \ln\frac{1}{z} - 3$ if $z \ll 1$.

E is the beam energy in the centre of mass system of the colliding beams and m_1, m_2 are the masses of the beam particles. Eqn(2) does not take into account, for the proton case, the effect of form factors. In Ref. (16) it is shown that for $\mu^+\mu^-$ production in $p\bar{p}$ collisions at 2E = 540 GeV the total virtual photon flux is reduced by a factor ~ 4 masses of 10 GeV and a factor of ~ 7 for masses of 20 GeV. For HERA these factors will be reduced to roughly $(4)^{\frac{1}{2}} = 2$ or $(7)^{\frac{1}{2}} = 2.6$ respectively. Most of this loss of flux occurs at large q^2 values. In the small angle tagging system at HERA considered below the maximum q^2 value is $\simeq 0.2(\mathrm{GeV/c})^2$. Parameterising the proton form factor as [19] :

$$\frac{1}{\left(1 + \frac{q^2}{0.7}\right)^2}$$

The maximum suppression factor expected is ~ 1.7. In order to give a realistic estimate of the tagging efficiency in the small angle region (Eqn 15 below) where form factor effects are small, the tagging efficiency is normalised to the total flux of transverse photons without form factor corrections. Multiplying this tagging efficiency by the total flux given by Eqn(2) then gives a good estimated of the tagged luminosity. I should be borne in mind however that due to the form factor effects the untagged luminosity may be, depending on the mass of the produced system, up to a

factor of two smaller than given by Eqn 2.

A more useful parameter for comparing different machines is the acceptance corrected luminosity given by :

$$\frac{d\mathcal{L}^{Acc}_{\gamma\gamma}}{dW} = \frac{d\mathcal{L}^{TOT}_{\gamma\gamma}}{dW} A(W,E,\theta_c) \ \ldots \qquad (3)$$

where $A(W, E, \theta_c)$ is an acceptance function which depends upon W,E and the lower polar angle limit θ_c for the acceptance of produced particles.

The precise definition of A will depend on the fraction of the solid angle in the CM system that is required to be observed. Consider the production of ultra-relativistic particles in the two photon collision at an angle θ in the lab system (Fig.3)

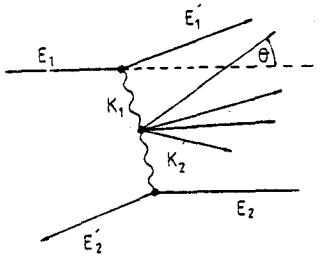

Fig. 3 - Kinematical definitions in the lab system.

For a given angular cut in the lab system : $\theta_c < \theta < \pi - \theta_c$ (a symmetrical detector is assumed) and a given range of production angles in the two photon centre of mass system : $\theta^*_1 < \theta^* < \pi - \theta^*_2$ (Fig. 4) there is a maximum boost given by the relativistic velocity β_c such that all particles produced in the indicated range of θ^* lie within the angular cut in the lab.

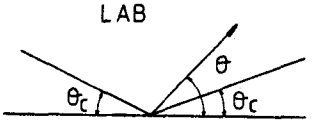

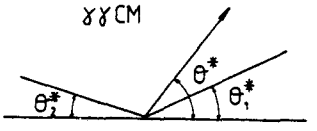

Fig. 4 - Angular acceptance intervals in the lab and γγ CM systems.

For fixed values of θ_c and θ^*_1 it is found that :

$$\beta_c = \frac{\cos\theta^*_1 \left[\sqrt{R(1 + (R-1)\cos^2\theta^*_1)} - 1\right]}{1 + R\cos^2\theta^*_1} \qquad (4)$$

$$\cos\theta^*_2 = \frac{(\gamma_c^2 - 1)\sin^2\theta_c + \cos\theta_c}{\gamma_c^2 \sin^2\theta_c + \cos^2\theta_c}, \quad R = \frac{\tan^2\theta^*_1}{\tan^2\theta_c}$$

Taking for example $\theta_c = 10°$ to correspond to the minimum angle in a solenoidal detector at which detection and momentum analysis by magnetic deflection is feasible, and $\theta^*_1 = 45°$ to have a reasonably large acceptance in the $\gamma\gamma$ centre of mass sytem it is found that :

$$y_c = \frac{1}{2} \ln \frac{(1+\beta_c)}{(1-\beta_c)} = 1.6 \ , \ \theta^*_2 = 6°$$

Acceptance = 72 % 4π in $\gamma\gamma$ C.M.

Here y is the laboratory rapidity of the $\gamma\gamma$ system. This can also be written in terms of the scaled energies of the two virtual photons $x_1 = K_1/E_1$, $x_2 = K_2/E_2$ (see Fig. 3) as

$$y = \frac{1}{2} \ln \frac{x_1}{x_2} \tag{5}$$

In Eqn (5) and in the following discussion the transverse motion of the $\gamma\gamma$ system is neglected.

The luminosity function L in Eqn (1) can be written, in either of the following differential forms :

$$\frac{d^2L}{dx_1 dx_2} = \left(\frac{\alpha}{\pi}\right)^2 \left(\ln\frac{2E}{m_1}\right)\left(\ln\frac{2E}{m_2}\right) \left[1+(1-x_1)^2\right]\left[1+(1-x_2)^2\right] \frac{1}{x_1}\,\frac{1}{x_2} \tag{6}$$

$$\frac{d^2L}{dydz} = 2\left(\frac{\alpha}{\pi}\right)^2 \left(\ln\frac{2E}{m_1}\right)\left(\ln\frac{2E}{m_2}\right) \left[1+(1-ze^{y})^2\right]\left[1+(1-ze^{-y})^2\right] \frac{1}{z} \tag{7}$$

where $z = W/2E$

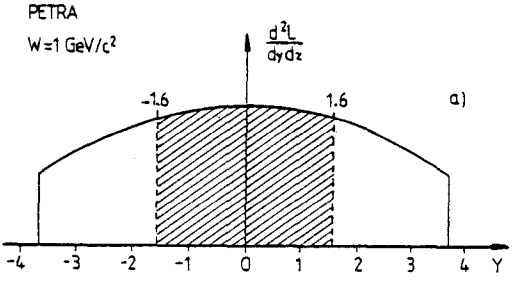

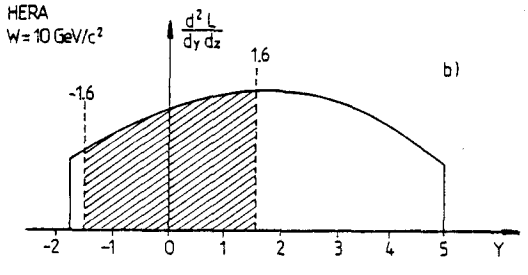

Note that x_1 and x_2 are invariant with respect to Lorentz transformations along the beam direction if the masses of the beam particles and the virtual photons are neglected. They thus have the same values in the lab, the colliding beam centre of mass system and the $\gamma\gamma$ centre of mass system.

The distribution of the luminosity function in terms of the laboratory rapidity of the $\gamma\gamma$ system is shown in Fig. 5a for PETRA with $W = 1.0\,GeV/c^2$ and in Fig. 5b for HERA with $W = 10\ GeV/c^2$. The shape of the rapidity distribution is similar in the

Fig. 5 - Differential luminosity function versus lab rapidity.
a) PETRA, E = 20 GeV W = 1 GeV/c²
b) HERA, E_e = 30 GeV, Ep = 820 GeV, W = 10 GeV/c². The cross hatched area indicates region accepted by the cuts $10° < \theta < 170°$, $6° < \theta^* < 45°$ for ultra-relativistic produced particles.

two cases, but for HERA the centre is displaced by $\simeq 1.6$ units of rapidity because of the boost between the lab and the ep centre of mass system. The region of accepted luminosity corresponding to the cuts defined above is cross hatched. It is clear that the boost between the lab and the overall centre of mass systems at HERA causes a small loss of acceptance in this case. Simply a different part of the rapidity distribution (corresponding to 2γ systems moving in the same direction as the incoming electron beam) is sampled. However, this is no longer true for larger masses $\geq 13\ \mathrm{GeV/c^2}$ when the acceptance defined by the rapidity cut $|y| < 1.6$, is limited to 50 %. This will be further discussed below. By integrating Eqn (7) over the accepted range of rapidity it is easy to obtain an analytical expression [28] for the acceptance function $A(W,E,\theta_c)$. Here, for simplicity, it is noted that the rapidity distributions are roughly flat so that :

$$A(W,E,\theta_c) = A(W,E,y_c) \simeq \frac{y_c}{y_{MAX}} = \frac{y_c}{\ln(\frac{1}{z})} \tag{8}$$

where Eqn. (5) and the relation :

$$z^2 = x_1\, x_2 \tag{9}$$

have been used.

To compare the energy (W) range of the different machines and to see in a clear way the effect of acceptance cuts it is particularly useful to use the Courau plot [29]. If x_1, $x_2 \ll 1$ Eqns (6) and (7) simplify to :

$$d^2L = K \times d\left[\ln(\frac{1}{x_1})\right] d\left[\ln(\frac{1}{x_1})\right] \tag{10}$$

or

$$= K' \times d\left[\ln(\frac{1}{z})\right]\, dy \tag{11}$$

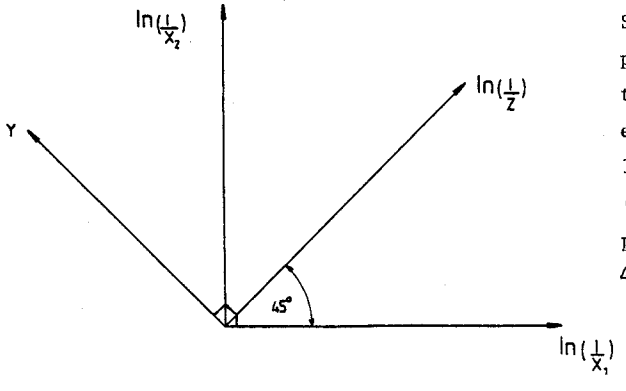

So the luminosity function is proportional, in this approximation, to the area in a plot of either $\ln(\frac{1}{x_1})$ versus $\ln(\frac{1}{x_2})$ or $\ln(\frac{1}{z})$ versus y. Using Eqns (5) and (9) it can be seen that these two plots are related to each other by a 45° rotation (Fig. 6).

Fig. 6 - The Courau Plot

As the effect of an angular acceptance cut translates naturally into a rapidity cut (Eqn (8) above) different angular cuts correspond to lines parallel to the diagonal of the $\ln(\frac{1}{x_1})$ versus $\ln(\frac{1}{x_2})$ plot. The kinematic range defined by the possible values of the mass of the 2 photon system, W, is delimited by straight lines perpendicular to the diagonal. The neglect of x_1, x_2 as compared to unity in Eqns (6) and (7) is only important near the extremes of the rapidity plateau (see Figs 5a,b) where the differential luminosity drops by a factor $\lesssim 2$ as compared to the centre. Figs 7,8 and 9 are Courau plots in which HERA is compared with, respectively, PETRA, LEP($\frac{1}{6}$) or SLC and LEP (2). Because of the boost between the overall centre of mass system and the lab the accepted region for HERA is displaced below the diagonal.

For masses less than $E_{CM}e^{-y_c} \simeq 13$ GeV/c^2 ($y_c = 1.6$) HERA loses little acceptance as compared to the e^+e^- colliders. However it is clear that for larger masses the acceptance is limited to 50 % as here the y_{MAX} allowed by kinematics is $< y_c$ and exactly the area below the diagonal is accepted. This results from the arbitary choice of y_c which is just equal to the rapidity difference between the lab and ep CM systems.

It is clear from Fig. 7 where PETRA ($E_{cm} = 40$ GeV) is compared with HERA $E_{CM} = 314$ GeV) that the effective energy range for two photon physics increases only very slowly with E_{CM}. The new kinematic region appears with only a relatively low luminosity. Fig. 10 indicates the great importance of forward acceptance for two photon physics. The Courau plot for HERA is shown with the acceptance regions corresponding to angular cuts θ_c of 2.6, 10°, 30° indicated separately. The 30° cut is typical of the first generation PETRA solenoïdal detectors. 2.6° corresponds to the minimum acceptance angle specified in the HERA proposal [27] . Also shown in Fig. 10 is the region accessible to a $\simeq 0°$ tagging system in the proton beam line, to be discussed below. It can be seen that tagging system covers the interesting high mass region from 10 to 40 GeV/c^2 with a good efficiency. It's acceptance is much worse in the low mass region from 1 to a few GeV/c^2 where the effects of diffractive electroproduction background to the 2γ process are expected to be most severe (see below).

The luminosity functions defined by Eqn 2 are shown in Fig. 11 for PETRA, LEP (1/6) or SLC, LEP(2) and HERA. LEP (1/6) corresponds to the probable first running configuration of LEP, with only 1/6 of the (conventional) R.F. power installed [30]. LEP (2) is the maximum energy machine that would result from full utilisation of superconducting R.F.

The acceptance functions given by Eqn (8) with $\theta_c = 10°$, $y_c = 1.6$ are shown for the different machines in Fig. 12. Fig. 13 presents the accepted two photon luminosities, given by Eqn (3), as a function of W for the different colliders. Effective ee or ep luminosities are taken from TABLE 2.

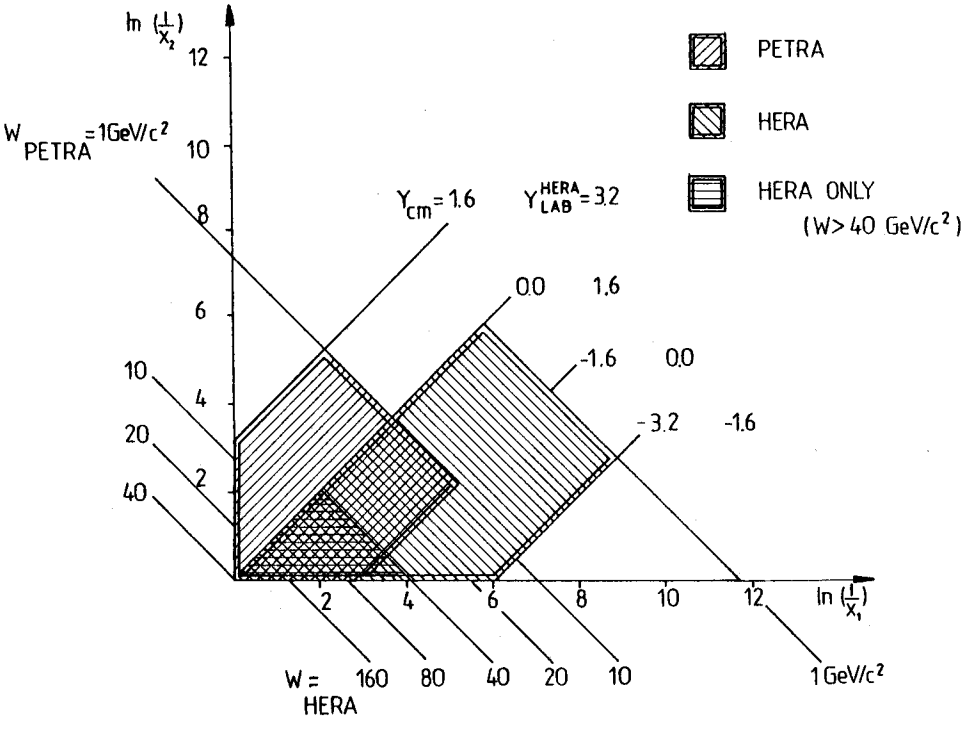

Fig. 7 - PETRA/HERA Comparison.

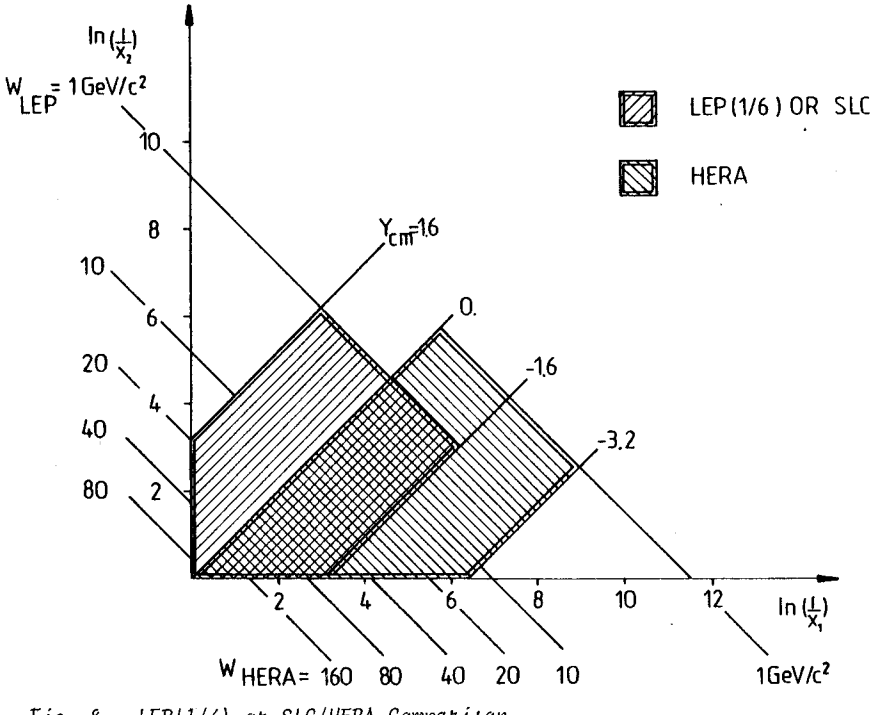

Fig. 8 - LEP(1/6) or SLC/HERA Comparison.

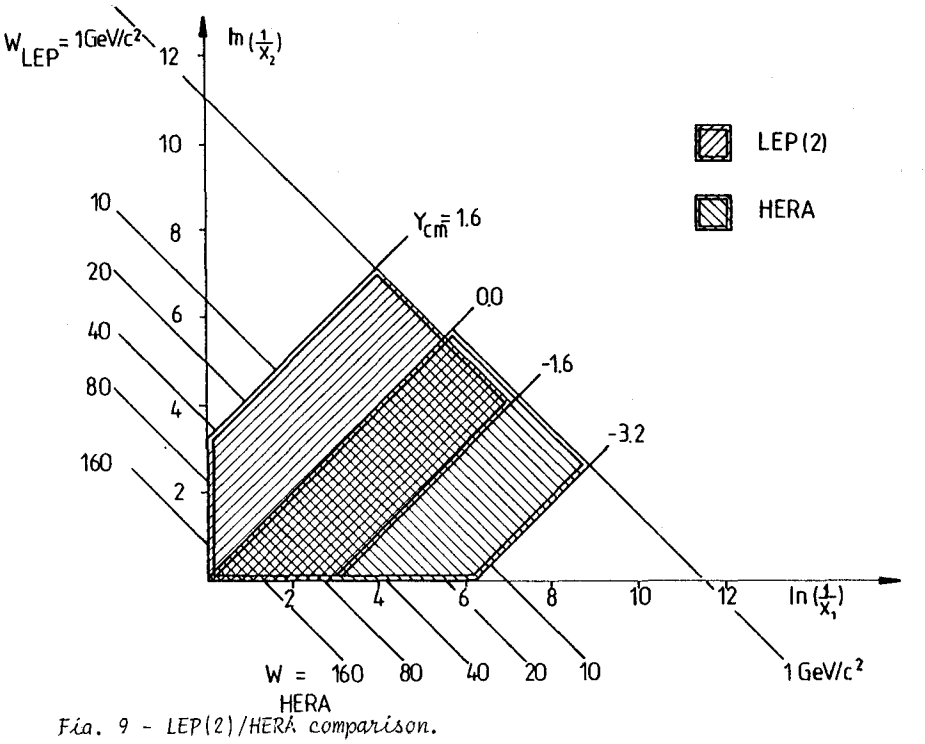

Fig. 9 - LEP(2)/HERA comparison.

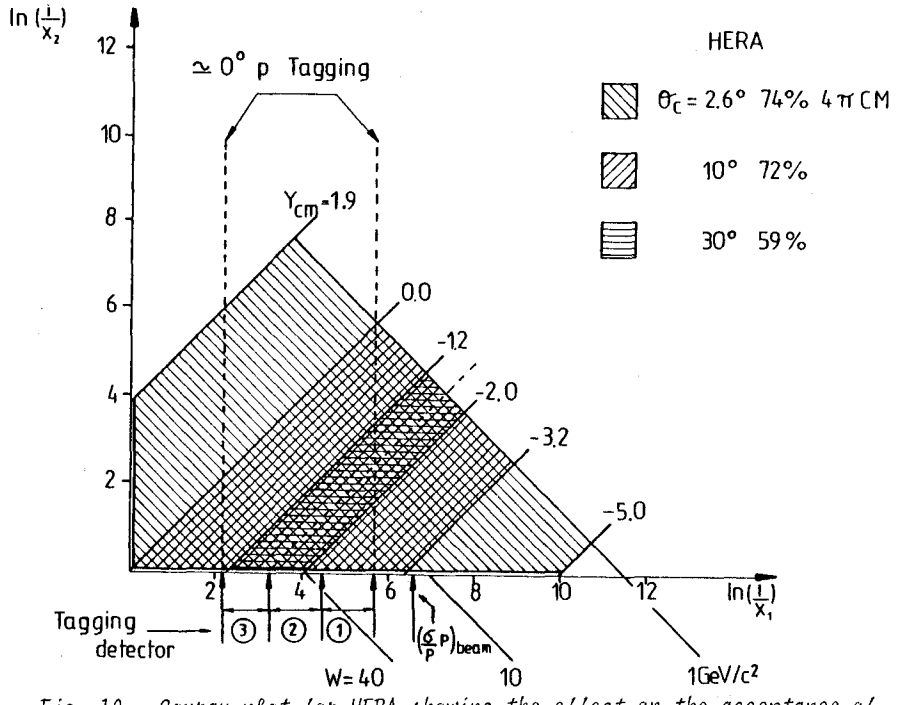

Fig. 10 - Courau plot for HERA showing the effect on the acceptance of different angular cuts, and the kinematical region covered by the proposed ≃0° proton tagger.

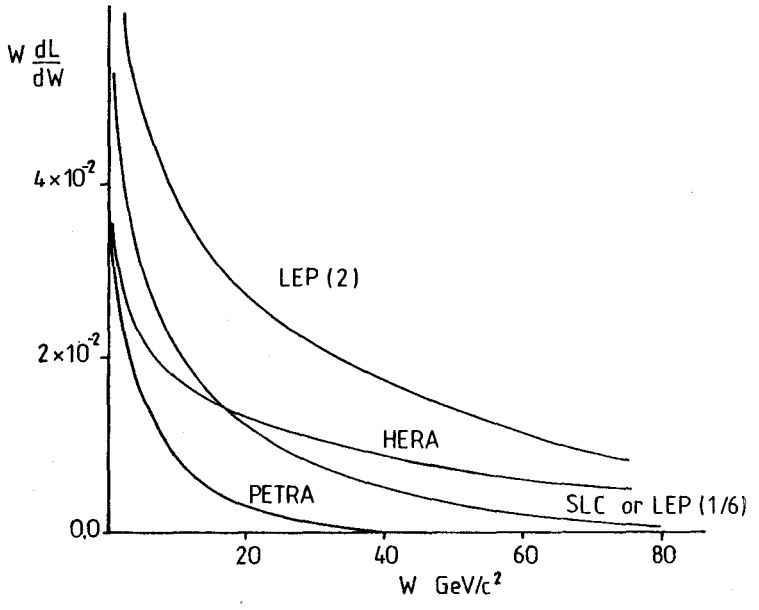

Fig. 11 - Differential luminosity functions for different colliders.

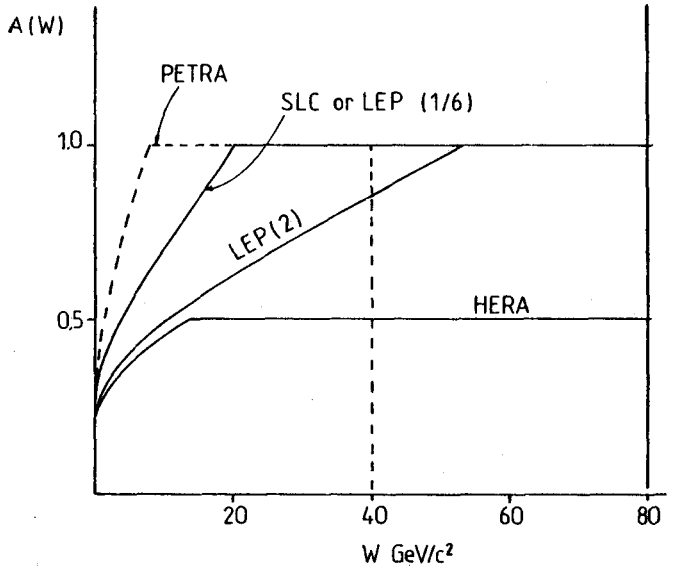

Fig. 12 - Acceptance function versus W for different colliders.
$10° < \theta < 170°$, $6° < \theta^* < 45°$, $y_c = 1.6$.

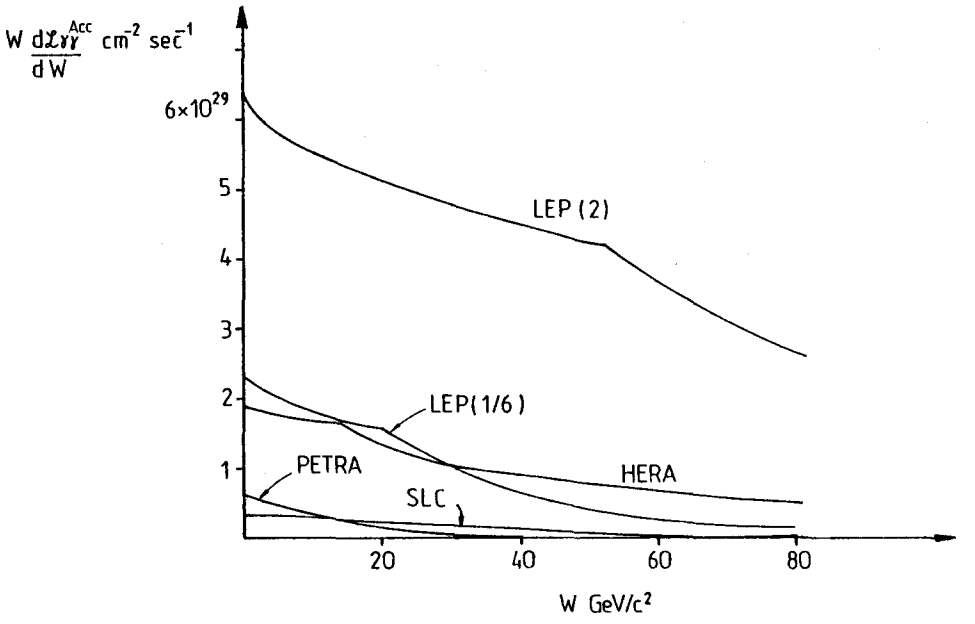

Fig. 13 - Accepted differential luminosity versus W for different colliders.

The following comments can be made on the basis of Fig. 11, 12, 13.

- SLC has a smaller luminosity than PETRA in the low mass region and seems of little interest for "classical" 2γ physics. Here however the interesting possibility of real $\gamma\gamma$ or γe collisions (see section 4 below) should not be forgotten.

- HERA competes very well with LEP (1/6) both from the viewpoint of intrinsic 2γ luminosity (Fig. 11) and effective luminosity (Fig. 13). In the energy region $W > 40$ GeV/c^2 HERA is clearly superior. Both HERA and LEP(1/6) give $\simeq$ 3X PETRA 2γ luminosity in the low mass region.

- LEP(2) is superior to HERA by a factor $\simeq 2$ in intrinsic luminosity (Fig. 11) and a factor ~ 3 in effective luminosity (Fig. 13). However taking into account the notorious difficulty that all e^+e^- machines have had till now to reach their design luminosity, and the possibility (still unknown) that the situation may be better for ep collisions the levels of the various curves in Fig. 13 should be treated with some scepticism. In practice, the relative positions of the LEP (2) and HERA curves could easily be reversed. In contrast the curves shown in Figs 11 and 12 are determined essentially by QED and kinematics and so are subject to a much smaller uncertainty.

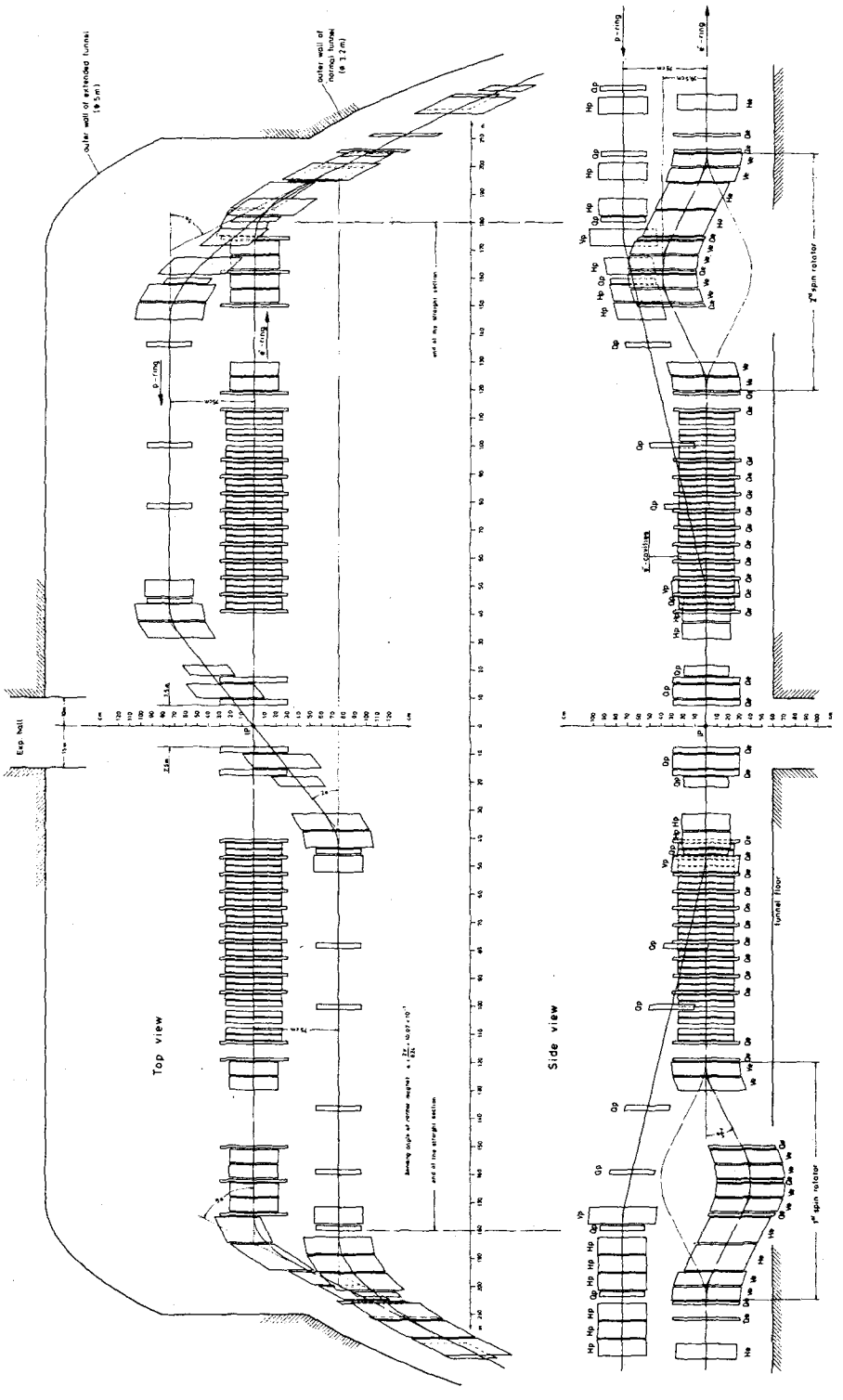

Fig. 14 - Layout of an interaction region at HERA.

The overall conclusion is that both HERA and the first generation LEP machines improve significantly over the existing machines PETRA and PEP (factor ~ 3 in 2γ luminosity at low masses). If LEP(2) reaches its design luminosity it will have almost an order of magnitude higher luminosity than existing machines at low masses. This luminosity will be useful however mainly for untagged physics, as is the case at existing machines. If LEP(2) does not reach design luminosity it will have a very serious competitor in the high energy region in HERA. In any case, as will be discussed in the following section, HERA has quite unique features which facilitate single or double tag two photon physics.

3. SMALL ANGLE TAGGING AT HERA

The beam transport system forseen [27] for a HERA interaction region is shown in Fig. 14. The 820 GeV proton beam crosses the 30 GeV $e^{\pm}$ beam horizontally at an angle of 20 mrad. Immediately after the beam crossing the proton beam is bent back parallel to the electron line by a horizontal bending magnet. It is this horizontal bend which makes possible $\simeq 0°$ tagging for the scattered protons.

Before discussing the tagging system in more detail some comments should be made on the kinematics of two photon collisions at HERA. Fig. 15 shows, in the ep CM system the configuration of an 2γ collision event resulting in the production of a system of mass 10 GeV/c^2 at rest in the lab system. The energies of the virtual photons radiated by the electron and proton are, respectively, 26.2, 0.96 GeV ($x_2 = 0.167$, $x_1 = 0.0061$). If y_{CM} is the rapididty difference between ep CM and the lab and θ_e, θ_p are the electron and proton scattering angles in the ep CM system, the corresponding angles in the lab system are :

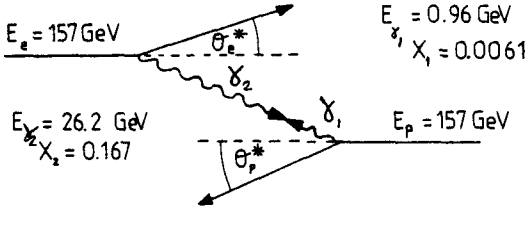

Fig. 15 - Kinematics of a typical 2 photon event at HERA in the ep CM system. W=10 GeV/c^2. The produced system is at rest in the lab.

$$\theta_e = \frac{\theta_e^*}{\gamma_{CM}(1-\beta_{CM})} = e^{y_{CM}}\,\theta_e^* = 5.0 \times \theta_e^*$$

$$\theta_p = \frac{\theta_p^*}{\gamma_{CM}(1+\beta_{CM})} = e^{-y_{CM}}\,\theta_p^* = 0.2 \times \theta_p^* \qquad (12)$$

Since, as pointed out above, $y_{CM} = 1.6$.

Eqns (12) imply that both small angle proton tagging (where protons are detected at angles $< \theta_{MAX}$) and finite angle electron tagging (where electrons are detected at angles $> \theta_{MIN}$) are more efficient than would be the case if the ep CM system were at rest in the lab :

	$y_{CM} = 0$	$y_{CM} = 1.6$
proton angular acceptance :	$0 < \theta < \theta_{MAX}$	$0 < \theta < 5\theta_{MAX}$
electron angular acceptance :	$\theta_{MIN} < \theta$	$0.2\theta_{MIN} < \theta$

The kinematical effects of the 20 mrad crossing angle are very small and so are neglected in Eqns[12].

If the protons are scattered at angles which are small compared to the angular divergence of the beam at the interaction point, which is given by [27]

$$\alpha_x = 3.9 \times 10^{-5} \text{ rad} \quad \text{(horizontal)}$$

$$\alpha_y = 9.0 \times 10^{-5} \text{ rad} \quad \text{(vertical)}$$

the trajectory of a proton with a given fractional energy loss x_1 can be simply calculated. The horizontal displacement at a given position in the machine is given by :

$$d = D_x x_1 \tag{13}$$

where D_x is the horizontal dispersion function. D_x in the proton beam line downstream of a HERA interaction region is shown in Fig. 16.

To have the greatest sensitivity to small values of x_1 the detector should be placed near to the maximum of D_x, which is about 100 m downstream of the interaction point. Other detectors, closer to the interaction point, where D_x is smaller will then be sensitive to larger values of x_1. The smallest value of x_1 which can be detected is limited by :

(i) The intrinsic energy spread in the proton beam :

$$\left(\frac{\sigma_p}{p}\right)_{beam} = 1.4 \times 10^{-3} \qquad [27]$$

(ii) The transverse beam dimension at the position of the detector .

If the detector is placed too close to the beam the lifetime of the latter will be

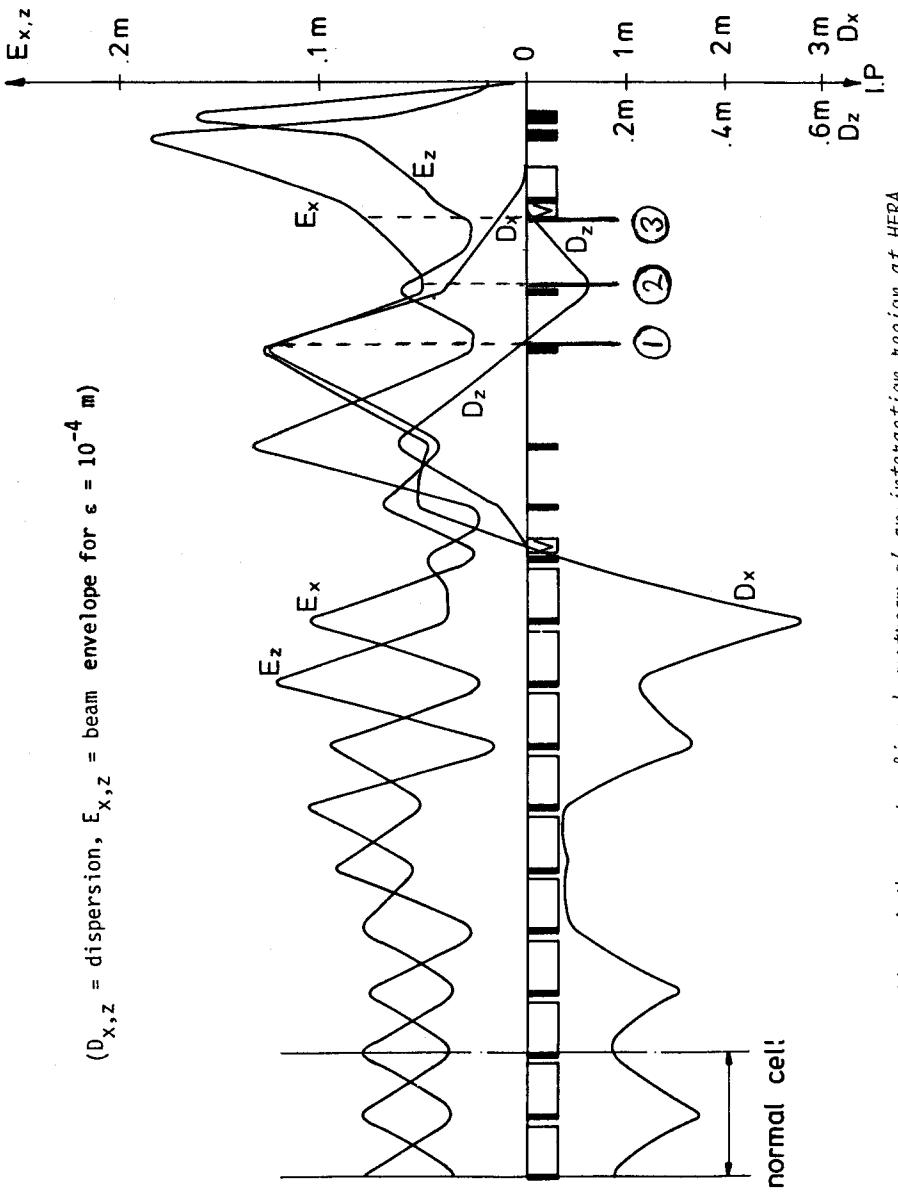

Fig. 16 - Beam optics of the proton line downstream of an interaction region at HERA. (1), (2), (3) indicate the locations of tagging detectors.

limited by interactions of the tails of the beam distribution with the detector. In practice the detector should not be closer to the beam than :

$$D_x \left(\frac{\sigma_p}{p}\right)_{beam} + n\sigma_x \qquad (14)$$

where σ_x = transverse beam size

$$= 0.069 \sqrt{E_x} \qquad (\sigma_x \text{ in mm, } E_x \text{ in m})$$

E_x is the horizontal beam envelope function shown in Fig. 16. n should be in the range 5-10 to ensure negligible beam losses.

The largest value of x_1 that can be detected for $\simeq 0°$ scatters is determined by the position of the downstream bending magnet and the radius (3cm) of the vacuum pipe. This last parameter can clearly be made more flexible by installing a special section of beam pipe of larger radius.

By placing 3 detectors at distances of 55 m, 75 m, and 100 m downstream of the interaction point it is possible to cover the range

$$0.0032 < x_1 < 0.11$$

in fractional proton energy loss (or scaled photon energy). Details on the parameters of the tagging detectors are given in TABLE 3.

A possible candidate detector is the Multi Electrode Silicon Detector (MESD) [31] which has the required property of operating easily in high vacuum conditions and could have a spatial resolution in the range 10-300 μ. A telescope of such detectors could mesure both the position and angle of the scattered protons. For protons scattered at 0° a 1mm spatial resolution corresponds to a precision in the fractional energy of the virtual photon of about 5% (see TABLE 3). The positions of the detectors in the lattice are shown in Fig. (16) and the corresponding ranges in the variable $\ln(\frac{1}{x_1})$ are shown in the Courau plot (Fig. 10). Also indicated in Fig. 10 is the value of $\ln(\frac{1}{x_1})$ corresponding to intrinsic beam energy spread $(\frac{\sigma_p}{p})_{beam}$. It is clear from Fig. 10 that the tagging is effective mainly in the high W-region when the angular acceptance for the produced final state particles is properly taken into account.

A realistic calculation of the tagging efficiency to be expected using a system such as that defined in TABLE 3 requires a study of particle tracking through the HERA beam elements.

Here a rough order of magnitude calculation is made by noting that the proposed system covers a range of horizontal scattering angles up to 0.54 mrad in the lab. An optimistic estimate of the tagging efficiency is given by assuming that for a given value of x_1 the whole angular range :

$$0 < \theta < \theta_{MAX}$$

is detected independant of the azimuthal angle of scattering. A more conservative estimate is given by assuming that only protons scattered through angles less than the horizontal beam divergence of 3.9×10^{-5} radians are detected. For comparison the inner edge of the furthest tagging detector and the beam line subtend an angle of 8.7×10^{-5} radians at the interaction point. The first estimate is optimistic because protons can be lost if they scatter in a direction opposite in azimuth to the sense of magnetic deflection, the second is conservative because the overall angular acceptance of the tagging system is underestimated.

The tagging efficiency corresponding to the above angular range in the lab system and fractional energy loss x_1 is given approximately by :

$$\varepsilon(0 < \theta < \theta_{MAX}) = \frac{\ln[r+1] - r/(r+1)}{\left[2\ln\left(\frac{2E}{m_p}\right) - \frac{1}{2}\right]} \qquad (15)$$

where

$$r = \left(\frac{5E\theta_{MAX}}{m_p x_1}\right)^2$$

This formula may be derived from the exact transverse luminosity function [28],[32] in the limit x_1, $\theta_{MAX} \ll 1$. The factor 5 comes from the boost between the ep centre of mass and the lab systems (see Eqns 12). The following values are found for the tagging efficiency :

	"Optimistic" $\theta_{MAX} = 0.54$ mrad		"Pessimistic" $\theta_{MAX} = 0.039$ mrad	
$x_1 = 0.0032$	0.8	(0.51)	0.33	(0.08)
0.01	0.59	(0.31)	0.14	(0.005)
0.10	0.19	(0.013)	4×10^{-4}	8×10^{-7}

It can be seen that the small angle tagging becomes ineffective for large values of the fractional energy loss x_1. This is because the peak in the angular distribution

of the scattered protons is at an angle of $\frac{x_1 m_p}{E}$ and so, for large x_1, is displaced far from the acceptance region of the tagging system. The figures in brackets indicate the tagging efficiency that would be obtained if the ep CM system were at rest in the lab i.e. the factor 5 in Eqn(15) is replaced by one. In the physically interesting region where :

$$0.0032 < x_1 < 0.01$$

covered by the tagging detectors 1 and 2 a tagging efficiency of > 40 % can be expected. In tagging detector 3 protons are detected with a somewhat lower efficiency (probably $\geq$ 10%) in the case that they are scattered at angles which are large as compared to the beam divergence.

With similar approximation to those used in Eqn(15) the electron tagging efficiency for the angular range :

$$\theta_{MIN} < \theta$$

can be written as

$$\varepsilon(\theta > \theta_{MIN}) = \frac{2 \ln 5 \left(\frac{2x_2}{\theta_{MIN}}\right) + \frac{1}{2}}{\left[2 \ln \frac{2E}{m_e} - \frac{1}{2}\right]} \qquad (16)$$

Some typical values are :

	θ_{MIN} = 45 mrad	θ_{MIN} = 20 mrad
x_2 = 0.037	0.18 (0.06)	0.24
0.167	0.30 (0.17)	0.36
1.0	0.43 (0.31)	0.50

The bracketed figures are found when the factor 5 in Eqn. (16) (coming from the boost to the ep CM system) is replaced by one.

45 mrad corresponds to the minimum detection angle defined in the HERA proposal [27] It can be seen that there is little gain in efficiency in reducing θ_{MIN} to 20 mrad. This is no longer true however when form factor effects are important (see below).

The tagging efficiencies for both protons and electrons are sufficiently large to make double tag physics viable. The kinematic configuration shown in Fig. 15 for

example has a double tag efficiency, even taking the "pessimistic" figure for the proton case, of ~ 10%. Depending on the physics, the naïve tagging efficiencies quoted above will be modified by form factor effects [4].

For a simple VDM type coupling of the photon, for example, a form factor of order

$$F(q^2) = \frac{1}{(1 + \frac{q^2}{m_\rho^2})^2} \qquad (17)$$

is expected. Because the q^2 values reached by the small angle proton tagging system are low $\lesssim 0.2(\mathrm{GeV}/c)^2$ the values of F are large at HERA $\gtrsim 0.6$. This may be compared to a value of 4×10^{-3} for tagging at 20 mrad at LEP(2). For electron tagging at HERA F has maximum values of 0.05, 0.36 for θ_{MIN} = 45,20 mrad. Smaller angle electron tagging than forseen in the current HERA proposal would therefore be advantageous for "soft" single tag and double tag two photon physics. It should be noted however that the simple VDM suppression factor 5 given above, which corresponds to the ρ propagator only is ~ 2 times smaller than the prediction of generalised vector meson dominance, where the effect of higher mass vector mesons are taken into account [4]. When the virtual proton couples to the hadronic system in a point like manner (as in photon structure function measurements, or processes where jets are produced at high p_T) no propagator suppression as in Eq. 17 is expected. HERA would be particularly suitable for a double tag measurement of almost real photons, using the virtual photons radiated by the proton beam as target, and those radiated by the electron beam as the probe. The relevant kinematical variables Q^2,x,y can be determined completely from the double tag measurements, avoiding the $x_{VIS} \rightarrow x$ unfolding problems which arise if only a single tag measurement is made. It is hard to see how LEP could compete for this type of measurement. The diffractive electroproduction process which can constitute a serious background for $\gamma\gamma$ physics at low W and q^2 values (see Section 4 below) would be expected to give a negligible contamination in a structure function experiment.

4. BACKGROUNDS TO TWO PHOTON PROCESSES AT HERA

The most serious background for hadronic states produced in two photon collisions at HERA (Fig. 17a) is likely to be the diffractive electroproduction process (Fig.17b).

Using the equivalent photon approximation for the eeγ and ppγ vertices in Fig. 17a

and for the eeγ vertex in Fig. 17b the observed cross section ratio, for production of a system X of mass W and rapidity y is estimated to be :

$$\frac{\sigma^{obs}_{2\gamma\to X}}{\sigma^{obs}_{\gamma p\to X}} = \frac{2}{W}\left(\frac{\alpha}{\pi}\right)\left[2\ln\frac{2E}{m_p} - \frac{1}{2}\right]\frac{\sigma_{\gamma\gamma\to X}(W)}{\frac{d\sigma^{diff}_{\gamma p\to X}}{dW}(W_{\gamma p},W)}\frac{\varepsilon_{2\gamma}(W,y)}{\varepsilon_{\gamma p}(W,y)} \qquad \ldots (18)$$

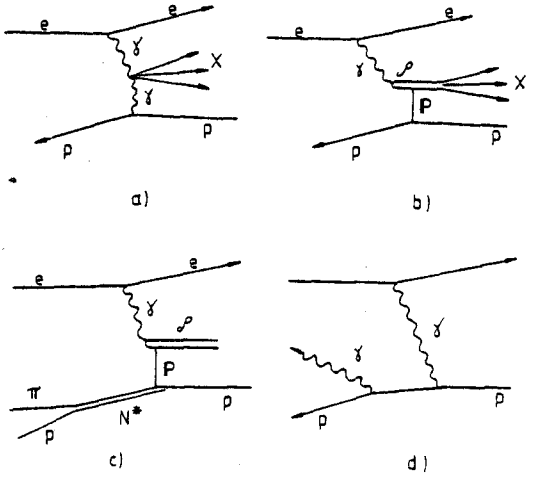

Fig. 17 - Signal and backgrounds in 2γ collisions at HERA. a) 2γ process. b) inelastic diffractive electroproduction. c) diffractive N^* electroproduction. d) beam beam bremsstrahlung.

Where $\sigma_{\gamma\gamma\to X}(W)$ is the total $\gamma\gamma$ cross section to produce system X with effective mass W, and $\frac{d\sigma^{diff}_{\gamma p\to X}}{dW}(W_{\gamma p},W)$ is the differential cross section to produce a system of mass W by diffractive photo production where $W_{\gamma p}$ is the total γp centre of mass energy. $\varepsilon_{2\gamma}$, $\varepsilon_{\gamma p}$ are the proton tagging efficiencies for the two photon and electroproduction process respectively.

One process where measurements exist for both 2γ production [33] and photoproduction [34] is the system $\pi^+\pi^+\pi^-\pi^-$ for masses W of 1.1 - 1.8 GeV/c^2.

It can be seen from Fig. 10 that masses as small as 1.5 GeV/c^2 are detected in the tagging system only for values of x_1 near to the minimum of 0.0032. This implies that $W_{\gamma p}$ = 26.3 GeV/c^2 when W = 1.5 GeV/c^2. Taking the $(E_\gamma^{lab})^{-0.4}$ dependance of the photoproduction cross section found in Ref. [34] it is estimated that :

$$\frac{d\sigma_{\gamma p\to 4\pi}}{dW} = 0.5\ \mu b/GeV/c^2 \quad (W_{\gamma p} = 26.3\ GeV/c^2,\ W = 1.5\ GeV/c^2)$$

while Ref. [33] gives

$$\sigma_{\gamma\gamma\to 4\pi} = 0.2\ \mu b \qquad (W = 1.5\ GeV/c^2)$$

Taking θ_{MAX} = 0.039 mrad, then as found above $\varepsilon_{\gamma 2}$ = 0.33. To calculate $\varepsilon_{\gamma p}$ it

is noted that, in this case [34]

$$\frac{d\sigma_{\gamma p \to 4\pi}}{dq^2} \simeq e^{-7q^2}$$

If $q^2_{MAX} \simeq 25\, E^2\theta^2_{MAX} << 1$ then

$$\varepsilon_{\gamma p} = \frac{\int_0^{q^2_{MAX}} e^{-7q^2}\, dq^2}{\int_0^{\infty} e^{-7q^2} dq^2} \simeq 7\, q^2_{MAX}$$

giving $\varepsilon_{\gamma p} = 6.6 \times 10^{-3}$

for $\theta_{MAX} = 0.039$ mrad.

So from Eqn(18)

$$\frac{\sigma^{obs}_{2\gamma \to 4\pi}}{\sigma^{obs}_{\gamma p \to 4\pi}} = 0.70 \qquad W = 1.5\ GeV/c^2$$

Because of the dependence of $\varepsilon_{\gamma p}$ on θ^2_{MAX} this ratio would be much smaller if a larger value of θ_{MAX} were used. Conversely a smaller value of θ_{MAX} would result in a sharp reduction in the electro production background, at some cost in tagging efficiency. It is clearly of importance to be able to measure accurately both the angle and the position of the scattered proton.

It is more difficult to give an estimate of the diffractive electroproduction background to be expected at higher masses, where the main physics interest at HERA lies. To make an estimate of the level of such background the kinematical configuration shown in Fig. 15 is considered.

It is assumed that the total inelastic diffractive cross section is the same as the elastic one (i.e. ρ,ω,ϕ production) $\simeq$ 10 μb and that $\sigma_{\gamma\gamma \to X}$ is 0.3 μb as given by VDM and factorisation argumements.

The distribution in W is taken to be flat :

$$\frac{d\sigma_{\gamma p \to X}}{dW} = \frac{10\ \mu b}{W_{\gamma p}} = \frac{10\ \mu b}{125\ GeV/c^2}$$

while the q^2 distribution is taken to be less steep [35] than in the low mass region above.

$$\frac{d\sigma_{\gamma p \to X}}{dq^2} \simeq e^{-5q^2}$$

giving $\varepsilon_{\gamma p} = 4.7 \times 10^{-3}$ with $\theta_{MAX} = 0.039$ mrad.

From Eqn (15) if is found that :

$$\varepsilon_{2\gamma} = 0.22$$

or using Eqn (18).

$$\frac{\sigma^{obs}_{2\gamma \to X}}{\sigma^{obs}_{\gamma p \to X}} = 0.91 \qquad W = 10\ GeV/c^2$$

Considering the conservative nature of the above assumptions, particularly the large assumed value for the inelastic diffractive cross section, and the flat W distribution (which surely overestimates the high mass region) this result is quite encouraging.

It should also be pointed out that for the most interesting final states in 2γ collisions accessible at high W values, for example deep inelastic scattering on an almost real photon, high p_T jet production, or exclusive production of high p_T meson pairs, the diffractive electro-production background is expected to be absent. In the high p_T processes there is another type of background coming from direct γ quark or γ gluon scattering where the quark or gluon is a constituent of the incident proton. Such events however (unlike the 2γ collisions where the same hard scattering pro processes may contribute) are always expected, as in the Drell Yan process, to be accompanied by a target fragmentation jet.

Requiring the detection of a scattered proton with very small scattering angle and energy loss should effectively suppress this background. Further rejection , can be obtained requiring the absence of fragmentation products accompanying the detected

proton, either in the forward hadronic calorimeters of the detector, or in special veto detectors with an acceptance extending down to smaller angles.

Another possible source of background are events where the proton is diffractively excited : $p \rightarrow N^*$ where N^* is a resonance with the same quantum numbers as the proton (Fig. 17c). It is not difficult to see, from simple kinematical arguments, that such processes are not expected to give significant backgrounds in the small angle tagging system. Considering for example : the lightest such resonance, the N^* (1410) the maximum possible energy for the decay proton is 154.8 GeV in the ep CM system giving $x_1 = 0.014$. Such events are therefore kinematically forbidden for tagging detector 1 . The rate in the other detectors should be low, as the typical (decay at $\theta^* = \frac{\pi}{2}$) decay angle and energy of the proton in the lab system are 0.72 mrad and 580 GeV ($x_1 = 0.29$) whereas the acceptance range of the tagging system is $\theta < 0.54$ mrad and $x_1 < 0.11$.

A potentially large source of background in the small angle tagging system is that due to the beam-beam bremstrahlung process where a photon is radiated from the proton line. One graph contributing to this process is shown in Fig. 17d . The cross section, differential in the fractional energy loss x_1 is given by [36] .

$$\frac{d\sigma}{dx_1} = \frac{2\alpha^3}{m_p^2 x_1} \left\{ 2\left[1 + (1 - x_1)^2\right] - \frac{4}{3}(1-x_1) \right\} \left[\ln \frac{4(1-x_1)E^2}{m_p^2 x_1} - \frac{1}{2} \right] \quad (19)$$

Taking the worst case, the minimum value of $x_1 = 0.0032$ and $\Delta x_1 = 0.001$ gives a cross section of :

$$5.2 \times 10^{-33} \text{ cm}^2$$

With a luminosity of $6 \times 10^{31} \text{cm}^{-2}\text{sec}^{-1}$ this corresponds to a total count rate of 0.3 hz. A more relevant parameter is the number of counts per bunch crossing which is 3×10^{-8}. Clearly there is no problem of occupation of the tagging detectors from this source. It is interesting to note, from Eqn (19) that if e^+e^- collisions under the same kinematic conditions are considered the rate would be a factor 6×10^6 higher, so there would be an occupation problem (0.18 hits per buch cross). At LEP with its lower duty cycle, (4 bunches instead of 210) the situation is even worse and it has been concluded [37] that there small angle tagging is not possible for angles below 1 mrad.

In summary, the rough calculations, presented in this section indicate that two photon physics at HERA should be distinguishable from backgrounds when the small angle

tagging system is used. In this connection it is important to measure both the position and the angle of the scattered photon with good precision, as the diffractive electroproduction background drops sharply at small scattering angles. For processes which have a characteristic two photon signature, less stringent angular cuts are needed. Beam beam bremstrahlung backgrounds (in sharp contrast to LEP and other e^+e^- machines) are negligible.

5. WEAK BOSON PRODUCTION AT HERA.

Before describing the technical realisation and the physics interest of real γe and $\gamma\gamma$ collisions it is interesting to note that a glimpse (or perhaps more) of the physics of the γe collision processes :

$$\gamma e^{\pm} \rightarrow W^{\pm}\nu \qquad \text{(i)}$$

$$\gamma e \rightarrow Z^{o}e \qquad \text{(ii)}$$

can already be obtained at HERA. The energy and luminosity of HERA is such that there should be a sufficient flux of high energy Weisacker-Williams photons radiated by the proton beam to observe both (i) [38] and (ii) [39] . In addition $W^{\pm}$ bosons can be produced via the process, specific to ep collisions [40] .

$$\gamma^{*}p \rightarrow W^{\pm} X^{o}_{++} \qquad \text{(iii)}$$

Where the γ^{*} is a virtual photon radiated by the electron beam.

At HERA with beam energies and effective luminosity as given in TABLE 2 the following cross sections and numbers of events can be expected for these processes :

	$\sigma_{tot}(cm^2)$	Ref.	Number of events (2 years at $\bar{\mathcal{L}}$)
$e^{\pm}p \rightarrow \nu W^{\pm}X^{+}$	9.0×10^{-38}	[38]	110
$e^{\pm}p \rightarrow e^{\pm}Z^{o}X$	1.0×10^{-36}	[39]	1300
$e^{\pm}p \quad e^{\pm}W^{\pm}X^{o}_{++}$	1.2×10^{-36}	[40]	1500

The cross sections quoted correspond to the standard Glashow-Weinberg-Salam electroweak theory. The estimate of Ref. [40] which uses a simple Weisacker-Williams formula to estimate the flux of virtual photons radiated by the $e^{\pm}$ is probably somewhat optimistic. There seems to be an inconsistency between ref. [38], [39] concerning

the relative contributions of the elastic and inelastic proton form factors to the virtual photon flux. For a total ep CM energy of order 300 GeV,Ref. [38] found roughly equal contributions, whereas Ref. [34] found, at the same energy that the elastic contribution was more than an order of magnitude smaller then the inelastic one. Until this discrepancy is resolved, the last two results quoted above should be treated with some caution. Putting aside this difficulty the number of events for these processes of $\gtrsim 1000$ should be adequate to identity the Z^o and $W^{\pm}$ by the clean,purely leptonic,decay signatures :

$$Z^o \rightarrow e^+e^-, \quad \mu^+\mu^-$$

$$W^{\pm} \rightarrow e^{\pm}\nu , \quad \mu^{\pm}\nu$$

As will be discussed further below the processes (i) and (iii) are of special interest because they are sensitive to the direct γW^+W^- coupling, i.e. the magnetic moment of the W boson.

6. REAL γe AND $\gamma\gamma$ COLLISIONS IN ONE PASS LINEAR COLLIDERS.

Linear Colliders

In order to reach significantly higher energies in e^+e^- collisions than will be provided by LEP, a new type of machine known as the one pass linear collider has been proposed by groups at SLAC [6] , [41] , [42] and Novosibirsk [7]. The idea is to make a head on collision of the beams of two electron-linear accelerators or of two bunches from the same linac . The cost of such a machine and its energy are roughly proportional to its length. In contrast the cost of a e^+e^- storage ring is roughly proportional to the square of the desired centre of mass energy. It has been pointed out that to achieve significantly higher energies than LEP a linear collider is a more economical proposition. The luminosity of such a machine is given by the expression :

$$\mathcal{L} = \frac{N^2 \nu_{REP}}{4\pi \sigma_x \sigma_y} \qquad (20)$$

where N is the number of particles per bunch,ν_{REP} the repetition frequency of the bunch collisions and σ_x, σ_y are the horizontal and vertical beam widths (gaussian profiles are assumed). ν_{REP} is much smaller in a linear collider than in an e^+e^- storage ring (ν_{REP} = 250 kHz, 50 kHz, 180 Hz for respectively PETRA, LEP, and S.L.A.C.). In compensation N is made very large and σ_x, σ_y as small as technically

possible. For the SLC project [6] , [41] , [42] it is planned to increase N by a factor $\gtrsim 50$ and values of σ_x, σ_y as small as 1 - 2 μm with a corresponding beam emittance of 3×10^{-5} rad.m are proposed. The enormous mutual focussing forces destroy the bunches during collision, but, in so doing, actually increase the luminosity by the so called 'pinch effect' [6] , [42] . The SLC projet at SLAC has two aims, first to build a collider capable of studying Z^0 physics at relativly low cost and secondly to act as a prototype for a more ambitious collider giving centre of mass energies of up to 1 TeV.

Fig. 18 which shows a schematic diagram of the VLEPP project at Novosibirsk gives an idea of how such a high energy collider might look. Only one half of the machine is shown. The operating cycle is as follows : After colliding the e^+e^- bunches in one or more interaction regions (11), a pulsed deflection magnet (9) and a spectrometer (18) deflect the beam into a helical undulator (12)where of the order of 1% of the total beam energy is radiated in the form of circularly polarised photons with $\simeq$ 10 MeV energy. After passing through the undulator the beam is deflected by bending magnets and is used either in a stationary target experiment (16) or is absorbed in a beam dump. The polarised photons strike a conversion target (14) producing a beam of longitudinally polarised electrons and positrons. After charge selection these particles are accelerated up to an energy of 1 GeV in an intermediate accelerator (2). The bunch length of 1 cm is stretched by a factor of $\simeq$ 10 in the debuncher (3) and the longitudinal polarisation in rotated into the transverse direction. After collecting the beam in the large acceptance storage ring (4) it is cooled down to the required low emittance value by radiation damping in the cooling ring (5). The transverse polarisation is maintained in (4) and (5) by the Sokolov-Ternov mechanism [43]. After cooling the beam passes into the buncher (6) where the bunch length is reduced to $\sim$ 1 cm and the polarisation is rotated back into the longitudinal direction. To complete the cycle the beam is accelerated to high energy in the linear accelerator (7), (8) and the whole process is repeated. An injector (1) provides the initial beam.

Such a machine can provide collisions between longitudinally polarised $e^{\pm}$ at energies up to and beyond 1 TeV with luminosities of 10^{32} $cm^{-2}sec^{-1}$. Many technical problems remain, however to be resolved [6],[7],[42]. Experience with the SLC, whose principles of operation are essentially the same as described above for VLEPP should indicate whether these problems can be overcome.

Another feature of such a machine is the possibility to convert, with high efficiency the polarised electron beams of one or both of the colliding linacs into a beam of polarised real photons [8] ,[9],[10] . The principle of operation of such a "photon accelerator" will now be brefly described.

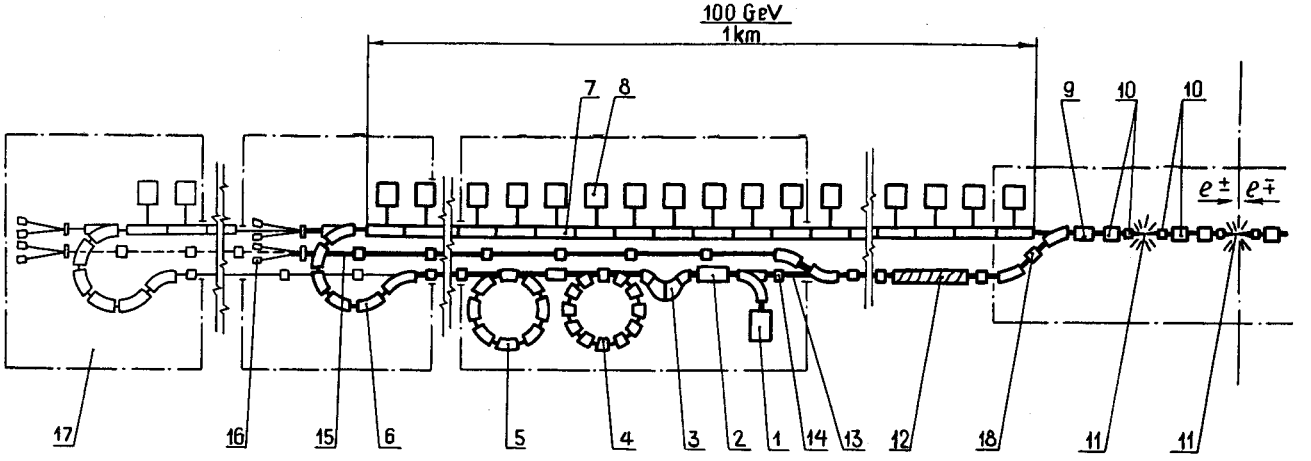

Fig.1

1. INITIAL INJECTOR
2. INTERMEDIATE ACCELERATOR
3. DEBUNCHER
4. STORAGE RING
5. COOLER -INJECTOR
6. BUNCHER
7. ACCELERATING SECTIONS
8. SHF SOURCE
9. PULSE DEFLECTOR
10. FOCUSING LENSES
11. COLLISION POINTS
12. HELICAL ONDULATOR
13. THE BEAM OF γ-QUANTA
14. CONVERSION TARGET
15. RESIDUAL ELECTRON BEAM
16. ELECTRON (POSITRON) BEAM EXPERIMENTS WITH STATIONARY TARGET
17. THE SECOND STEP
18. SPECTROMETER

Fig. 18 - The VLEPP project.

Compton Back Scattering

The production of high energy photons by collisions of highly relativistic particles with light quanta of optical wave lengths was first calculated by Feenberg and Primakoff [44] in an astronomical context. They considered the interaction of high energy cosmic electrons with starlight quanta.

The interest of such a process for high energy physics experimentation was pointed out, after the advent of the laser, by Milburn [45] and Arutyunian and Tumanian [46] One experiment, in which a polarised photon beam produced by Compton back scattering of a ruby laser was incident on a hydrogen bubble chamber was carried out some 15 years ago [47] .

The definition of kinematic quantities is given in Fig. 19. In addition the following dimensionless variables are introduced (the notation of Ref. [10] is followed)

$$y = \omega/E \qquad y_o = \omega_o/E$$

$$x = \frac{4y_o}{\gamma^2}\cos^2\frac{\alpha_o}{2} = \frac{4E\omega_o}{m_e^2}\cos^2\frac{\alpha_o}{2}$$

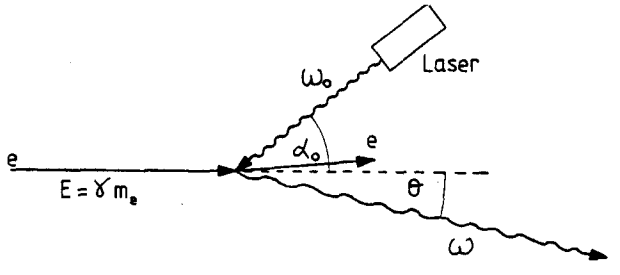

Fig. 19 - Kinematics of Compton back-scattering.

Taking typical values E = 50 GeV, ω_o = 1.17 eV (neodymium glass laser) and α_o = 0 x is found to be 0.90. For this case the energy of the incident photon in the electron rest frame is low $\simeq$ 0.12 MeV and the total scattering cross section is close to the classical (Thompson) limit of 2.5×10^{-25} cm^2.

The maximum energy of scattered photon is given by :

$$y_{MAX} = x/(1+x) \qquad (21)$$

while the energy of the scattered photon is related to its scattering angle θ by the relation ($\theta \ll 1$)

$$y = \frac{y_{MAX}}{1 + (\theta/\theta_o)^2} \qquad (22)$$

where $\theta_o = \sqrt{1+x}/\gamma$

High energy photons are scattered at angles smaller than $\theta_o \simeq \frac{1}{\gamma}$. The parameters a_e, a_γ and b are defined in Fig.20. a_e is the half width of the collision region of the electron beams. a_γ is the corresponding parameter for the laser and electron beams, while b is the distance from the electron electron beam collision point to the laser electron beam collision point. For both SLC and VLEPP $a_e \simeq 1$ to 2 μm, $a_\gamma \simeq 20$ μm and b is 5 to 10 cm. A transverse magnetic field B of order 1 T is need to deflect the electron beam after the laser crossing region to avoid direct electron electron interactions of the residual beam.

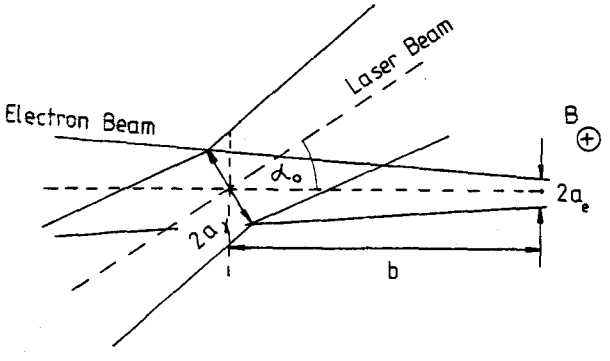

Fig. 20 - Definition of beam parameters for Compton backscattering of a laser beam.

The order of magnitude of the laser power needed to convert ~ 100 % of the electron beam into photons can be readily calculated. If S is the cross sectional area of the interaction region of the electron and laser beams, and n the number of photons in the laser pulse, saturation of the Compton scattering process will be reached if

$$n\sigma_c = S \tag{23}$$

Taking $\sigma_c = 2.5 \times 10^{-25}$ cm^2 and $S = \pi a_\gamma^2$ where $a_\gamma = 20$ μm gives $n = 5 \times 10^{19}$. The corresponding energy in the laser pulse, taking $\omega_o = 1.17$ eV is then 5.9×10^{19} eV or 9.4 joules. The efficiency of conversion of the electron beam into photons is measured by the coefficient k, which gives the γe and γγ collision luminosities in terms of the electron electron luminosity :

$$\mathcal{L}_{\gamma e} = k\mathcal{L}_{ee} , \qquad \mathcal{L}_{\gamma\gamma} = k^2\mathcal{L}_{ee}$$

The energy spectrum of the scattered photons for various values of E is shown in Fig. 21 for $\omega_o = 1.17$. As can be seen from Eqn 21, the higher the beam energy the closer is the end point of the scattered photon spectrum to the electron beam energy. The differential luminosity for γγ collisions, as a function of the mass of the produced system for the same series of E values is shown in Fig. 22. In Figs 23 and 24 the differential luminosity for eγ and γγ collisions respectively for E = 150 E = 150 GeV, $\omega_o = 1.17$ eV are compared with the corresponding luminosity expected from the virtual Weisacker-Williams photons radiated at the same energy. Even with k values as low as 30 %, the luminosity available in the real γγ collisions near the

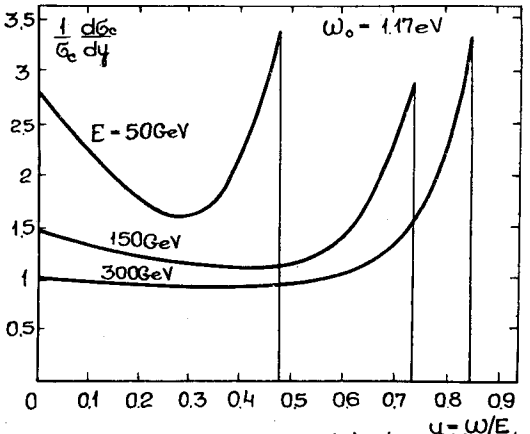

Fig. 21 - Energy spectrum of back scattered photons.

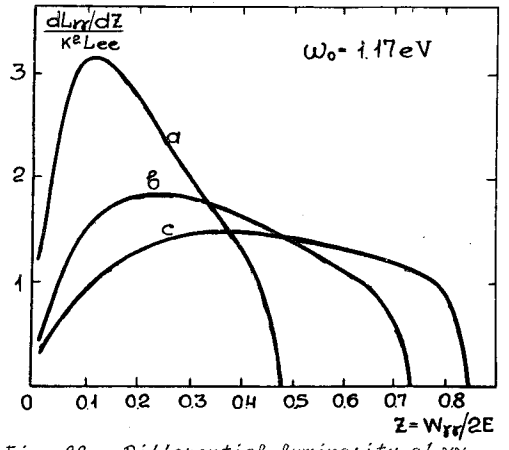

Fig. 22 - Differential luminosity of $\gamma\gamma$ collisions for $\rho^2 \ll 1$. Curves a,b,c correspond to E = 50,150,300 GeV.

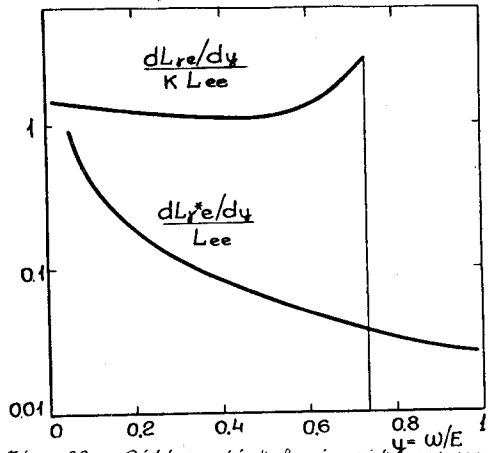

Fig. 23 - Differential luminosity for γe and $\gamma^* e$ collisions E=150 GeV, ω_o = 1.17 eV, $\rho^2 \ll 1$.

kinematical end point is some two orders of magnitude larger than in the virtual $\gamma\gamma$ collisions ! It can be seen from Eqn 22, that if photons are selected at small scattering angles to the incident electron beam, the energy spectrum will be concentrated more in the region of y_{MAX}, giving a photon beam with a narrower energy spread. Such a "monochromatisation" of the colliding beams can be most easily obtained by increasing b (Fig.20). If however the ratio :

$$\rho = \left(\frac{b\theta_o}{a_e}\right)^2 \qquad (24)$$

becomes large, the typical scattering angle of the photon (θ_o) is greater than the angular extent of the ee collision region as seen from the e laser interaction point (a_e/b) and aloss of luminosity results, even for the high mass region. This effect is demonstrated in Figs 25 and 26 where the differential luminosity functions for $e\gamma$ and $\gamma\gamma$ collisions respectively are shown for different values of ρ . It can be seen that monochromaticity is bought only at the cost of luminosity. If the laser photons have polarisation (circular or linear) this polarisation is largely retained by the scattered photons. If the laser light is unpolarised and the electrons are longitudinally polarised, the scattered photons have a high degree of circular polarisation. Details of these polarisation effects may be found in Ref. [10] .

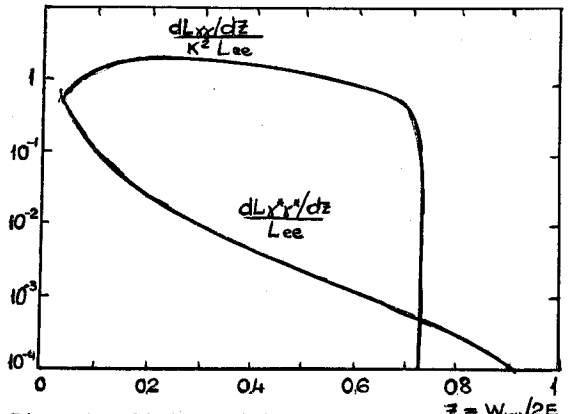

Fig. 24 - Differential luminosity for $\gamma\gamma$ and $\gamma^*\gamma^*$ collisions. E = 150 GeV, ω_o = 1.17 eV, $\rho^2 << 1$.

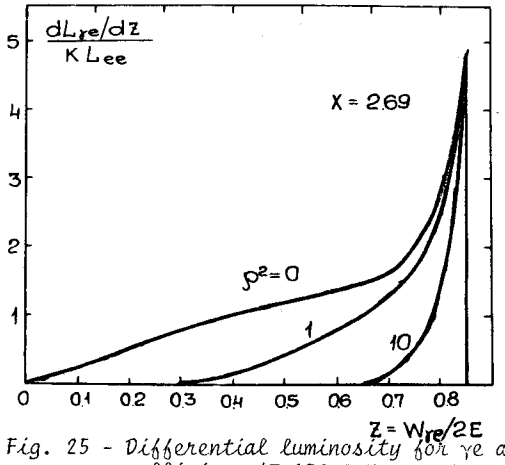

Fig. 25 - Differential luminosity for γe and $\gamma^* e$ collisions (E=150 GeV, ω_o=1.17 eV) for different ρ^2 values.

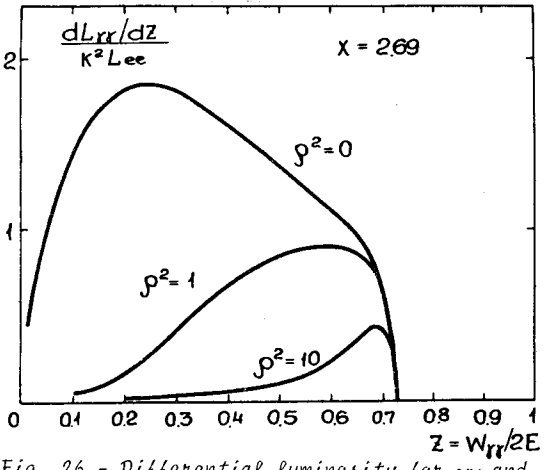

Fig. 26 - Differential luminosity for $\gamma\gamma$ and collisions (E=150 GeV, ω_o=1.17 eV) for different ρ^2 values.

The required laser power seems to be within the reach of existing technology. The outstanding problem is the high power output which is required in combination with a relatively high repetition rate. (180 Hz for SLC, 10 Hz for VLEPP). To date considerably higher power outputs have been achieved but at low repetition rates, and the required repetition rates or greater have been reached, but with somewhat lower power [10]. The required pulse length of 100 ps seems less difficult to obtain. A possible solution to the power and repetition rate problem would be to use a battery of 10 or 100 lasers of lower power, triggered in co-incidence.

A particularly elegant solution for the laser is proposed in Ref. 48. This is to place an undulator, or free electron laser in the early part of the linac (Fig. 27.). To provide sufficient laser power this needs to have a field of 2T, a period λ_o of 20 cm and a total length of 40 m. After passing through the undulator, the electron beam (energy 10 GeV) is diverted into a by-pass line (B in Fig. 27) so that the pulse of laser light arrives at the correct time, in advance of the electron bunch, to be focussed on to the opposing bunch. This system has the advantage that synchronisation of the laser beam collision is garanteed both in terms of arrival time and of pulse overlap. It is unfortunately not applicable to a one linac colli-

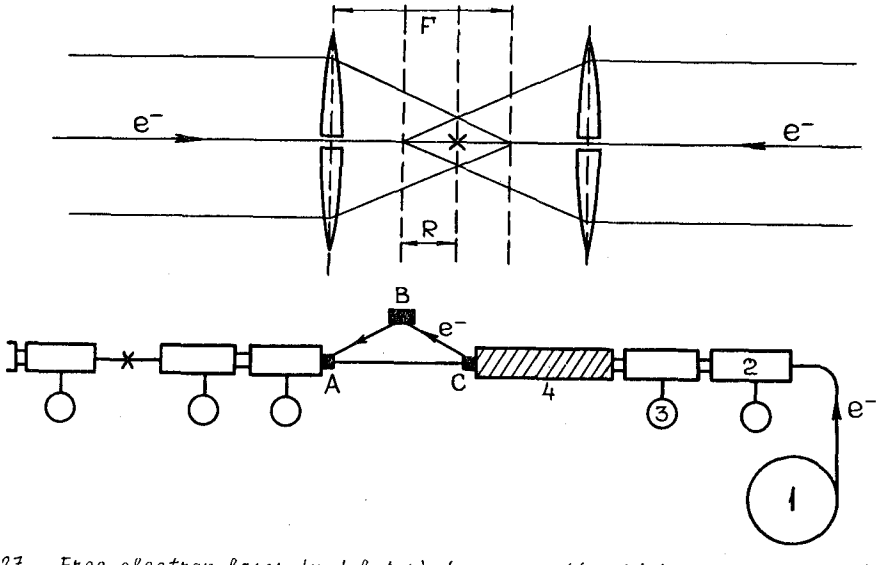

Fig. 27 - Free electron laser (undulator) for generating high energy photon beams. 1. - injector, 2. - accelerating system. 3. - High frequency generator. 4. - undulator.

der der such as the SLC, where magnetic bending is needed to bring the bunches into collision.

The problem of calibration of the luminosity of real $\gamma\gamma$ collisions has been considered at Novosibirsk by Kuraev, Schiller and Serbo [49]. At the very high energies of VLEPP traditional QED processes such as :

$$\gamma\gamma \rightarrow \mu^+\mu^-$$

$$\gamma\gamma \rightarrow e^+e^-$$

are not suitable, both because of the low value of the cross section and its rapid $(1/W^2)$ energy dependance. It is proposed to use instead the reaction :

$$\gamma\gamma \rightarrow e^+e^-\mu^+\mu^-$$

which has a larger, energy independant, cross section of 5.7×10^{-39} cm^2 and relatively clean signature due to the presence of a low mass muon pair which carries almost the full energy of one of the colliding photons. Special muon pair detectors in the forward direction will be required to observe this process.

7. THE PHYSICS OF REAL γe AND γγ COLLISIONS.

The advantage of real γe and γγ collisions, in luminosity terms, as compared to the "classical" 2γ physics using virtual photons is clear from Figs 23 and 24. Many of the most interesting processes from the theoretical viewpoint - those where QCD predictions can be tested - require large centre of mass energies in order to be in the kinematical region where perturbative calculations should be valid. Examples of such processes are the production of high p_T quark and gluon jets [50 , 51] or of pairs of mesons at high p_T[52] . Another advantage of the real γ beams is that they can be produced in various polarisation states (circular or transverse) so that more refined tests of theoretical predictions can be made. A good example of this is measurement of the real photon structure function, where by using longitudinally polarised electrons, and photons in arbitary circular or transverse polarisation states all the photon structure functions can, in principle, be measured. Even at the lowest beam energy proposed for VLEPP, E = 150 GeV, total centre of mass energies, in eγ collisions, comparable to those that will be attained at HERA in ep collisions should be obtained. In this case the contributions of Z^0 exchange to the photon structure function Fig. 28a and the corresponding W exchange process with ν production Fig. 28b should be measurable. At SLC with E = 50 GeV, the maximum q^2 in real eγ collisions is $\simeq 10^4 (\mathrm{GeV/c})^2$ where γ and Z^0 exchange contributions are already comparable but it is doubtful if the luminosity will be adequate to exploit this possibility.

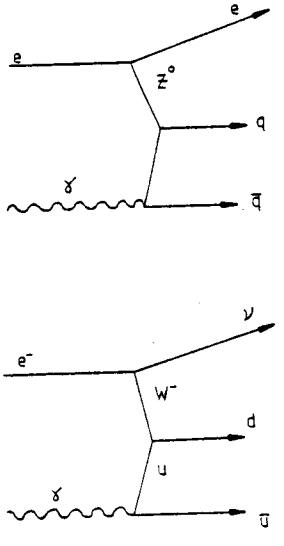

Fig. 28 - a) Z^0 exchange contribution to the photon structure function.
b) Charge current interaction on a photon target.

A particularly important field of physics that will be opened to experimental study by real γe and γγ collisions at high energy is the production of the gauge bosons Z^0, $W^{\pm}$.

The process $e^+e^- \rightarrow W^+W^-$ has been studied in some detail in connection with the LEP project [53] . Although, in principle, sensitive to the fundamental gauge couplings γW^+W^-, $Z^0W^+W^-$, it is in fact difficult to observe these contributions because the cross section is dominated by the neutrino exchange graph. In contrast the processes $\gamma e \rightarrow W\nu$ and $\gamma\gamma \rightarrow W^+W^-$ enable the couplings γW^+W^- and $\gamma\gamma W^+W^-$ to be directly measured. A brief discussion of gauge boson production in γe and γγ collisions follows.

$\gamma e \to Z^o e$

The differential cross section for this process is given in Ref. [13]. The total cross section as a function of the γe centre of mass energy, and the lowest order diagrams which contribute are shown in Fig. 29. The total cross section is [14]:

$$\sigma(\gamma e \to Z^o e) = \frac{\tilde{\sigma}}{x}\left[(1-\frac{2}{x}+\frac{2}{x^2})\,L + \frac{1}{2}(1-\frac{1}{x})(1+\frac{7}{x})\right]$$

where $x = (W_{\gamma e}/M_Z)^2$

$$\tilde{\sigma} = \frac{\pi\alpha^2}{2M_Z^2 \sin^2 2\theta_W}\left[1 + (4\sin^2\theta_W - 1)^2\right] = 5.9 \text{ pb}$$

$$L = 2\ln\left(\frac{W_{\gamma e}^2 - M_Z^2}{m_e W_{\gamma e}}\right) \qquad (25)$$

No fundamentally new couplings are measured in this process. The cross section is however large just above threshold. The dominant graph at high energy is u channel electron exchange, which results in emission of the Z^o preferentially antiparallel to the incoming photon direction.

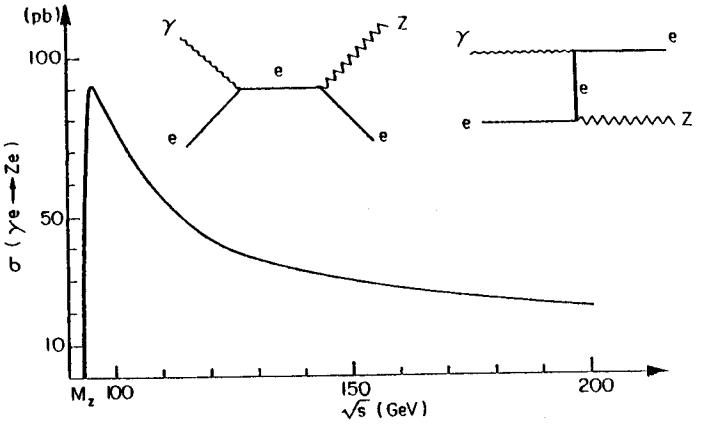

Fig. 29 - Cross section for the process $\gamma e \to Z^o e$ as a function of $W_{e\gamma} = \sqrt{s}_{e\gamma}$ and lowest order contributing graphs.

$\gamma e \to W^{\pm} \nu$

This process is discussed in Ref. [13], [14]. The lowest order diagrams and the total cross section versus $W_{e\gamma}$ are shown in Fig. 30. t channel W exchange gives an important contribution which is sensitive to the gauge coupling $\gamma W^+ W^-$. At high energies the W exchange graph is predominant and the produced W boson is emitted mostly parallel to the incoming photon. The total cross section can be written in terms of the degrees of longitudinal polarisation of the electron and photon beams $P^{\ell}_{e^{\mp}}$, P^{ℓ}_{γ} as [14]:

$$\sigma(\gamma e^{\mp} \to W^{\mp} \nu) = (1 \mp P^{\ell}_{e^{\mp}})(\sigma^{np} + P^{\ell}_{\gamma} \tau)$$

$$\sigma^{np} = \tilde{\sigma}\left[(1 - \frac{1}{x})(1 + \frac{5}{4x} + \frac{7}{4x^2}) - \frac{1}{x}(2 + \frac{1}{x} + \frac{1}{x^2}) \ln x\right]$$

$$\tau = \frac{\tilde{\sigma}}{x}\left[\frac{x-1}{4x}(13 + \frac{3}{x}) - (1 + \frac{3}{x}) \ln x\right]$$

$$\tilde{\sigma} = \frac{\pi \alpha^2}{M_W^2 \sin^2 \theta_W} = 47 \text{ pb}, \quad x = (W_{\gamma e}/M_W)^2 \qquad (26)$$

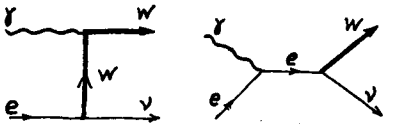

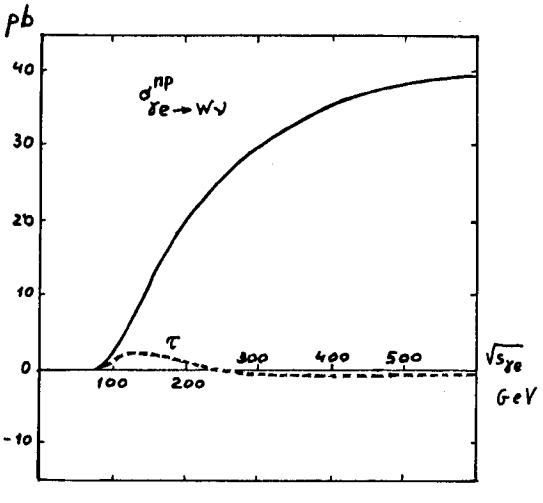

Fig. 30 - Cross section for the process $\gamma e \to W_{\nu}$ as a function of $W_{e\gamma} = \sqrt{s_{e\gamma}}$ and lowest order contributing graphs.

The cross section vanishes for right handed electrons and left handed positrons. τ is half the difference between the cross sections for photons with right handed and left handed polarisation. This is perhaps measurable in the region near threshold (see Fig. 30).

$\gamma\gamma \rightarrow W^+W^-$

Several theoretical calculations of this process have been made [14] ,[54] , [55] [56]. The total cross section can be written as [14] :

$$\sigma(\gamma_1\gamma_2 \rightarrow W^+W^-) = \sigma^{np} + P^{\ell}_{\gamma_1} P^{\ell}_{\gamma_2} \tau^a + \frac{1}{2} P^{t}_{\gamma_1} P^{t}_{\gamma_2} \tau \cos 2\Delta\phi$$

$$\sigma^{np} = \tilde{\sigma} v \left[1 + \frac{3}{16x} + \frac{3}{16x^2} - \frac{3}{16x^2} \left(1 - \frac{1}{2x}\right) L \right]$$

$$\tau^a = \frac{\tilde{\sigma} v}{16x} \left[-19 + \left(8' - \frac{5}{x}\right) L \right]$$

$$\tau = \frac{3}{16} \frac{\tilde{\sigma} v}{x^2} \left[1 + \frac{1}{2x} L \right]$$

where $\tilde{\sigma} = \frac{8\pi\alpha^2}{M_W^2} = 86$ pb $\quad x = (W_{\gamma\gamma}/2M_W)^2$

$$v = \sqrt{1 - \frac{1}{x}} \qquad L = \frac{1}{v} \ln \frac{1 + v}{1 - v} \tag{27}$$

Here $P^{\ell}_{\gamma_i}$, $P^{t}_{\gamma_i}$ are the degrees of longitudinal and transverse polarisation respectively of the photon i. $\Delta\phi$ is the azimuthal angle between the planes of transverse polarisation of the two photons. τ and τ^a can also be written in the form :

$$\tau = \sigma_{\parallel} - \sigma_{\perp}$$

$$\tau^a = \frac{1}{2} (\sigma_o - \sigma_2) \tag{28}$$

where $\sigma_{\parallel}$, $\sigma_{\perp}$ are the cross sections for photons with parallel, perpendicular planes of transverse polarisation and σ_o, σ_2 are the cross sections for states of total helicity 0,2 for the two photons. Fig. 31 shows the dependance of $\sigma^{np}, \tau, \tau^a$ on $W_{\gamma\gamma}$ as well as the 3 lowest order diagrams (all involving fundamental couplings of gauge bosons) which contribute to the cross section. It can be seen from Fig. 31 that the effects of longitudinal polarisation can be more easily measured than these of transverse polarisation. Such a measurement is sensitive to the different contributions of the γW^+W^- and the $\gamma\gamma W^+W^-$ couplings (Fig. 31).

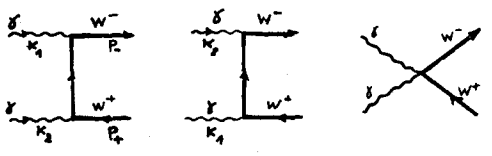

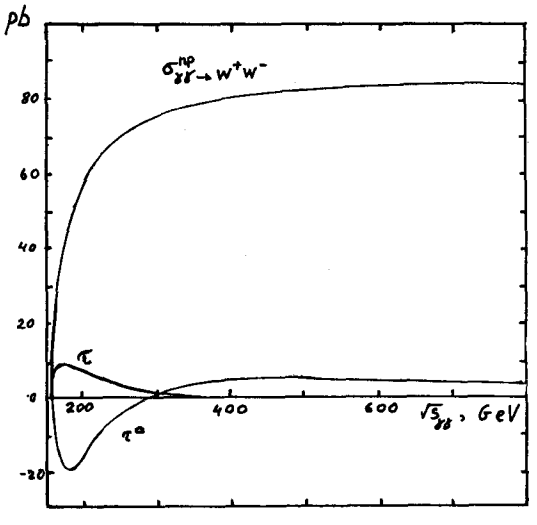

Fig. 31 - Cross section for the process $\gamma\gamma \to W^+W^-$ as a function of $W_{\gamma\gamma} = \sqrt{s}_{\gamma\gamma}$ and lowest order contributing graphs. For definitions of τ, τ^a see text.

$\gamma\gamma \to H \to Z^oZ^o$

In the case that the Higgs scalar meson of the standard electroweak theory is very heavy, the above process with a cross section of $\simeq 10^{-2}$pb is expected to be the dominant one for the process $\gamma\gamma \to Z^oZ^o$ [14]. This reaction would be a particularly clean way to detect a the Higgs scalar in this region, since unlike the reaction $\gamma\gamma \to H \to W^+W^-$ there is no "born term" corresponding to $W^\pm$ exchange.

The total cross section to be expected for the processes discussed above, when account is taken of the energy spectrum of the real photons produced by Compton back-scattering, are shown in Fig. 32. The cross sections shown are averaged over the energy distribution of the scattered electrons :

$$\frac{1}{N_\gamma}\frac{dN_\gamma}{dy} = \frac{2\pi\alpha^2}{xm_e^2\sigma_c(x)}\left[\frac{1}{1-y} + 1 - y - \frac{4y}{x(1-y)} + \frac{4y^2}{x^2(1-y)^2}\right] \qquad (29)$$

where x, y are defined in section 6 above, $\sigma_c(x)$ is the Compton cross section, and a laser photon energy of 1.17 eV is chosen. x is $\simeq 1$ for SLC energies and $\simeq$ 2-5 for VLEPP. In the curves corresponding to γe and $\gamma\gamma$ collisions a conversion efficiency k of 0.5 is assumed. Some counting rate estimates using Fig. 32 for SLC and VLEPP taking in each case 2 years of "effective luminosity" are presented in TABLE 4. Notice that for SLC the effective luminosity is now a factor 3 smaller than in TABLE 2, since the "pinch effect" enhancement is no longer operative. It should be remarked in general however that the parameters for optimum luminosity in γe and $\gamma\gamma$ collisions are not the same as in e^+e^- [7], implying that the estimates of TABLE 2 are perhaps conservative. For SLC the maximum [6] beam energy of 70 GeV is taken.

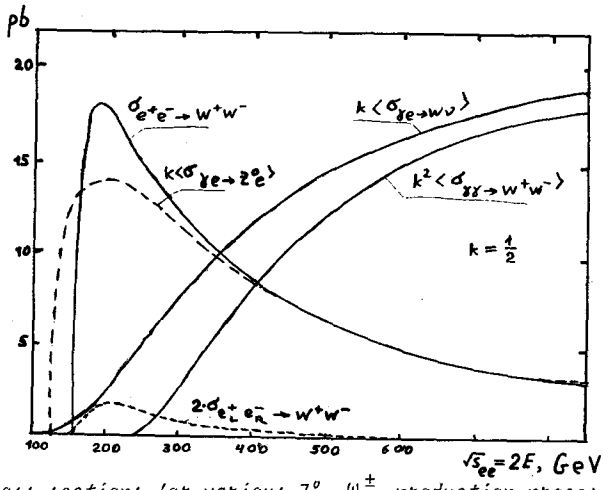

Fig. 32 - Cross sections for various Z^o, $W^{\pm}$ production processes, weighted by the photon energy distribution of Eqn(29) as a function of $2E = \sqrt{s_{ee}}$.

8. SUMMARY

A comparative study of the 2γ physics potential of PETRA, SLC, LEP(1/6), LEP(2) and HERA has been made. On the basis of the quoted design luminosities, both HERA and LEP (1/6) (the initial version of LEP with 50 GeV beams) offer a significant advantage in terms of accepted luminosity over the current (PETRA, PEP) generation of e^+e^- storage rings. LEP(2) (the ultimate version of LEP with superconducting R.F. and 130 GeV beams) will permit an order of magnitude increase in accepted luminosity over PETRA and PEP, in the low energy region as well as giving useful counting rates at 2γ masses as high as 100 GeV/c^2. Because of technical limitations on the acceptance of tagging detectors and background problems LEP (2) will be best used for untagged physics.

The SLC seems to be of little interest for virtual 2γ physics because of its rather low luminosity. The above statements are conditional on the respective machines reaching their design luminosities. Taking into account the difficulty all e^+e^- machines have experienced in approaching their design luminosity, it may well be that HERA will approach or even surpass LEP(2) for untagged two photon physics. In any case HERA seems to offer quite unique possibilities for single tag physics when the scattered proton is detected at very small angles. A first look at the background from diffractive electroproduction indicates that it should be less than or of the order of the rate from 2γ collisions. Even at 0^o the expected background level from beam-beam bremsstrahlung is negligible. The production of Z^o and $W^{\pm}$ bosons in γ e and γ p collisions should be observable at HERA.

In the more distant future a single pass linear collider such as VLEPP or a higher energy successor to the SLC could provide intense real photon beams by Compton back scattering of laser light. Such photon beams (which can be circularly or transversely

polarised) will enable real $\gamma\gamma$ and γe collisions to be observed at centre of mass energies as high as 1 TeV. Electroweak interference in the photon structure function as well as copious production of Z^o and $W^{\pm}$ via the reactions :

$$\gamma e \rightarrow Z^o e$$

$$\gamma e^{\pm} \rightarrow W^{\pm}\nu$$

$$\gamma\gamma \rightarrow W^+W^-$$

is to be expected. The last two reactions are sensitive to the fundamental gauge couplings γWW, $\gamma\gamma WW$.

ACKNOWLEDGEMENTS

I should like to thank A. Courau for a clarifying discussion on the calculation of tagging efficiency and J.M. Levy for valuable comments on the experimental results on diffractive photoproduction.

The material in sections (6) and (7) is drawn almost entirely from material provided directly to me by our colleagues in Novosibirsk. I thank them for their promptness in transmitting the information to me, and apologise to them for any errors or omissions in the account given above of their work.

HIGH ENERGY COLLIDERS

Machine	Colliding Beams (Energy in Gev)	Design Luminosity ($cm^{-2}sec^{-1}$)
CERN $\bar{p}p$	270 p + 270 $\bar{p}$	10^{29}
SLC	50 $e^{\pm}$ + 50 e^{-}	6×10^{30} (*)
	possibly $e^{\pm}$ + 30 γ	3×10^{29} (†)
	30 γ + 30 γ	4.5×10^{28} (†)
LEP ($\frac{1}{6}$) (**)	50 e^{+} + 50 e^{-}	4×10^{31}
LEP (2) (††)	130 e^{+} + 130 e^{-}	10^{32}
HERA	30 $e^{\pm}$ + 820 p	6×10^{31}
FNAL $\bar{p}p$	1000 p + 1000 p^{-}	10^{30}
ISABELLE pp	400 p + 400 p	10^{33}
VLEPP	$e^{\pm}e^{-}$	10^{32}
	$e^{\pm}\gamma$	
	$\gamma\ \gamma$	
	All beams polarised	
	Energy range 150 → 500	

(*) A factor 3 enhancement from the "pinch effect" assumed.

(†) Monochromatic γ beam with $\Delta E/E \simeq 0.1$ Ref. [8]

(**) 1st Stage of LEP

(††) Superconducting R.F. required.

Table 2

ENERGIES AND EFFECTIVE LUMINOSITIES FOR PETRA, LEP SLC AND HERA

Machine	PETRA	LEP ($\frac{1}{6}$)	LEP (2)	SLC	HERA
Colliding beam	20 e^{+}	50 e^{+}	130 e^{+}	50 $e^{+}(e^{-})$	820 p
Energies (GeV)	20 e^{-}	50 e^{-}	130 e^{-}	50 e^{-}	30 $e^{\pm}$
W_{MAX} (GeV/c)	40	100	260	100	314
$\bar{\mathcal{L}}$ ($cm^{-2}sec^{-1}$)	4×10^{30}	1.3×10^{31}	3×10^{31}	2×10^{30}	2×10^{31}

Table 3

PARAMETERS OF SMALL ANGLE TAGGING DETECTORS

Detector	1	2	3
Distance from interaction point (m)	100	75	55
Distance of detector from beam line (mm)	$8.7 < r < 30$	$8.9 < r < 30$	$10.5 < r < 30$
Effective distance of inner edge from beam	$D_x(\frac{\sigma_p}{p})_{beam} + 6\sigma_x$	" " $+ 28\sigma_x$	" " $+ 18\sigma_x$
D_x (m)	2.7	0.8	0.28
σ_x (mm)	0.86	0.28	0.5
Acceptance in x_1	$0.0032 \rightarrow 0.011$	$0.011 \rightarrow 0.0375$	$0.0375 \rightarrow 0.11$
$\frac{<\sigma_{x_1}>}{x_1}$ for $\sigma_r = 1$ mm	0.057	0.053	0.048

Table 4

COUNTING RATE ESTIMATES FOR Z°, $W^\pm$

PRODUCTION IN γe, $\gamma\gamma$ COLLISIONS AT SLC AND VLEPP

SLC E = 70 GeV $\bar{\mathcal{L}}^{(\dagger)} = 6.7 \times 10^{29}$ cm^{-2} sec^{-1}

VLEPP E = 150 GeV $\bar{\mathcal{L}}^{(\dagger)} = 3.3 \times 10^{31}$ cm^{-2} sec^{-1}

Numbers of events for 2 years at $\bar{\mathcal{L}}$

	SLC	VLEPP
$\gamma e \rightarrow Z^\circ e$	504	23,000
$\gamma e^\pm \rightarrow W^\pm \nu$	24	15,000
$\gamma\gamma \rightarrow W^+W^-$	-	4,000

(†) The effective luminosity $\bar{\mathcal{L}}$ is $\frac{1}{3}$ the quoted design luminosity. No "pinch effect" enhancement is included for the SLC.

DISCUSSION

Q. - Vermaseren

In a reaction ep → e$\mu\mu$ p vs ee → ee$\mu\mu$ most of the HERA advantage for tagging goes away when the observation of both μ's is demanded. See for instance NIKHEF preprint H/82-15.

A. - J.H.F.

This remark is true only for electron tagging. If a hadronic system is produced rather than muon pairs, the smaller form factor suppression will favour HERA over LEP. LEP cannot compete with HERA for the $\simeq 0°$ tagging as both technical acceptance limitations and beam-beam bremsstrahlung background forbid tagging at angles less than $\simeq$ 2 mrad at LEP.

Q. - Brodsky

There is an interesting hadronic diffractive process which would be a potential background to $\gamma\gamma$ physics in ep collisions ; specifically γ + pomeron → X or γ + (gg) → X where the proton scatters elastically and forward at large x_F. This is an interesting process to study in itself ; careful studies are needed to see if the $\gamma\gamma$ reactions are separable.

A. - J.H.F.

There is some data for the corresponding reaction in pp collisions (Fig. 2) which indicates, perhaps rather surprisingly, that "pomeron pomeron" collisions are rather ineffective in the production of low mass, low multiplicity systems. For the ep collisions however, I agree, diffractive electroproduction is a potentially important background. In the written version of the talk I shall try to make some estimate of its magnitude relative to the 2 photon process.

Q. - Jönsson

I would like to point out that the possibility of making 0°-tagging in principle also exists at DORIS, where the beams are vertically bent at some distance from the interaction point ; however, if you investigate the background situation you find that you will have problems with the beam beam single bremsstrahlung processes, which even if they don't contribute to the double tag rather directly will give a high single tag rate. To get around this problem you have to introduce an angular cut at about 1 mrad, which reduces the background by more than a factor 100.

If we wouldn't have these background problems the double tag efficiency at DORIS would be of the order of 25% but with a cut at 1 mrad it comes down to about 8% which still is quite impressive.
I suppose you have to worry about the same background problems at HERA as at DORIS.

A. - J.H.F.
Again, in the written version of the talk I shall give an estimate of the beam-beam bremsstrahlung background for tagging at HERA.

Q. - Wacker
I found in a study of 0° tagging at DORIS, that a measurement of position and angle of the scattered particle behind the bending magnet does not always give a unique solution, there are sometimes two possible tracks with different momenta and scattering angles. This is due to the quadrupoles in the beam line. In case of e beams, a shower counter can resolve this, but that is obviously impossible with protons.

A. - J.H.F.
Such ambiguities may also exist at HERA. If there is a sufficiently large difference between the proton momenta in the two solutions, the ambiguity can perhaps be resolved by observation of the produced final state. For exclusive final states measurement of the visible energy and rapidity define the energies of both virtual photons.

Q. - Kessler
I come back to Stan Brodsky's objection concerning $\gamma\gamma$ collisions at HERA. Actually we gave up studying $\gamma\gamma$ physics at HERA, because it came out from discussions with strong interaction specialists that - even tagging the proton at 0° - $\gamma\gamma$ reactions would be dominated by an overwhelming background from γ Pomeron collisions. As I understand, the experiment you mention is showing that the Pomeron is not there in double peripheral reactions ?

A. - J.H.F.
The ISR experiment shown in Fig. 2 can be interpreted in terms of conventional Regge exchanges only. There is certainly no "dominance" of double pomeron exchange in this experiment, in which the total centre of mass energy is 23 or 30.7 GeV. This has already been pointed out by H. Sens at the 1981 Paris photon-photon colloquium.

REFERENCES

1) L. Camilleri, J.H. Field, E. Gabathuler and G. Preparata, CERN 76-18 P169 Geneva 1976.

2) J.H. Field and P. Landshoff. Proceedings of the LEP Summer Study, CERN 79-01 P553 Geneva 1979.

3) ECFA-LEP Working Group Progress Report 1979, ECFA/79/39 P145.

4) J.H. Field in Proceedings of the International Workshop on $\gamma\gamma$ collisions. Amiens, France 1980. Lecture Notes in Physics 134 Springer Verlag 1980 P248.

5) M. Davier in Proceedings of the Fourth International Colloquium on Photon Photon Interactions Paris 1981. World Scientific Singapore (1981) P411.

6) B. Richter SLAC-PUB-2854 November 1981.

7) A. Siderov in Proceedings of 1981. International Conference on Lepton and Photon Interactions at High Energies. Bonn 1981, Ed. W. Pfeil, P944.

8) C. Akerlof. University of Michigan, pre-print UM HE 81-59 1981.

9) I.F. Ginzburg, G.L. Kotkin, V.G. Serbo and V.I. Telnov. Novosibirsk pre-print 81-50 1981.

10) I.F. Ginzburg, G.L. Kotkin, V.G. Serbo and V.I. Telnov. Novosibirsk pre-print 81-102 1981. Nuclear Instruments and Methods (in Print).

11) A.M. Kondratenko, E.V. Pakhtusova and E.L. Saldin. Novosibirsk pre-print 81-85 1981.

12) P. Kessler.Seminar on Gamma-Gamma Physics Paris 1982. Collège de France pre-print LPC/82-14 P61.

13) F.M. Renard,Z. Phys. C14(1982) 209.

14) I.F. Ginzburg. G.L. Kotkin, S.L. Panfil. and V.G. Serbo. Novosibirsk pre-print TP-3(127) 1982.

15) A. Donnachie (As 5) above P303.

16) C. Tao. As 5) above P281.

17) C. Carimalo, P. Kessler and J. Parisi. Phys. Rev. D18(1978) 2443.

18) R. Moore Z. Phys. C14 (1980) 351.

19) B. Schrempp and F. Schrempp, Nucl. Phys. B182 (1981) 343.

20) S. Drell and T.M. Yan Phys. Rev. Lett. 25 (1970) 316.

21) F. Vannucci as 4) above P238.

22) J.A.M. Vermaseren. NIKHEF (Amsterdam) preprint, NIKHEF-H/82-15.

23) C. Carimalo, P. Kessler and J. Parisi, Orsay 2 Photon Seminar 1981.
Orsay pre-print LAL 82/03 and College de France pre-print LPC 81-30.

24) Comment by H. Sens (see Ref. 5) P301.

25) J.C.M. Armitage et al. Phys. Lett. 82B (1979) 149.

26) G. Coignet, As 4) above P399.

27) DESY-HERA 81/10 July 1981

28) J.H. Field Nucl. Phys. B168 (1980) 477. Erratum B176 (1980) 545.

29) A. Courau. as 4) above P19.

30) The LEP "Pink book" CERN/ISR-LEP/79-33.
August 1979 and Ref. 4) above.

31) S.R. Amendolia et al. Physica Scripta 23 (1981) 674.

32) Ch. Berger and J.H. Field. Nucl. Phys. B187 (1981) 585.

33) See talk of H. Kolanoski at this workshop.

34) D. Aston et al. Nucl. Phys. B189 (1981) 15.

35) D. Aston et al. Nucl. Phys. B166 (1981) 1.

36) G. Altarelli and B. Stella.Lettre al Nuovo Cimento 9(1974) 416.

37) ECFA-LEP Working Group 1979. Progress Report. Ed. A. Zichichi ECFA/79/39 P161

38) H. Neufeld Z. Phys. 17C (1983) 145.

39) P. Salati and J.C. Wallet. Z. Phys. 16 C(1982) 155.

40) A.N. Kamal, J.N. Ng. and H.C. Lee. Phys. Rev. 24 (1981) 2842.

41) W. Panofsky as 7) P957.

42) H. Wiedemann SLAC-PUB-2849 November 1981.
A.A. Sokolov and I.M. Ternov, Sov. Phys. TETP 4(1957) 369.

43) and Sov. Phys. Doklady 8 (1964) 1203.

44) E. Feenberg and H. Primakoff.Phys. Rev. 73 (1948) 449.

45) R.H. Milburn.Phys. Rev. Lett. 10 (1963) 75.

46) F.R. Arutyunian and V.A. Tumanian. Phys. Lett. 4(1963) 76.

47) J. Ballam et al. Phys. Rev. Lett. 23 (1969) 498.

48) A.M. Kondratenko, E.V. Pakhtusova and E.L. Saldin.
Novosibirsk preprint 81-85 1981.

49) E.A. Kuraev, A. Schiller and V.G. Serbo.
Novosibirsk pre-print 82-107 1982.

50) S.J. Brodsky, T. de Grand, J. Gunion and J. Weis. Phys. Rev. D19 (1979) 1418.

51) K. Kajantie and R. Raito. Nucl. Phys. B159 (1979) 528.

J.H. Field, E. Pietarinen and K. Kajantie, Nucl. Phys. B171 (1980) 377.

52) S.J. Brodsky and G.P. Lepage. Phys. Rev. D24 (1981) 1808.

53) W. Alles, C. Boyer and A.J. Buras. Nucl. Phys. B119 (1977) 125.

54) K.J. Kim and Yung-Su Tsai. Phys. Rev. D8 (1973) 3109.

55) G. Tupper and M.A. Samuel. Phys. Rev. D23 (1981) 1933.

56) M. Katuya. Phys. Lett. 124B (1983) 421.